FEUP FACULDADE DE ENGENHARIA
UNIVERSIDADE DO PORTO

Evaluation of isoniazid and rifampicin on the biophysical properties of the membrane studied with 3D model systems

Ana Sofia Gomes Marques da Silva

Mestrado Integrado em Bioengenharia

Dissertação submetida para obtenção do grau de

Mestre em Bioengenharia – Ramo de Engenharia Biomédica

Porto, July 2013

This thesis was supervised by:

Prof. Dra. Salette Reis

Marina Pinheiro

Realized in:

U.PORTO

FACULDADE DE FARMÁCIA
UNIVERSIDADE DO PORTO

Research group:

requimte
rede de química e tecnologia

GABAI
Grupo de Análises Bioquímicas Ambientais e Industriais

“All our dreams can come true,
if we have the courage to pursue them.”
- Walt Disney

ACKNOWLEGMENTS

In this small space that is reserved, I must pay my gratitude and sincere acknowledgments to all those who helped and motivated me in the course of my work.

Firstly, I would like to thank professor Dr. Maria de La Salette Reis for all the knowledge shared and support granted, for her kindness and patience in helping me resolving my K_p "problem" as well as her availability in answering all my questions and concerns. Thanks for all these moments with you.

I would also like to thank to MSc Marina Pinheiro (about becoming a Dr.) for all the knowledge shared, accessibility in answering all my questions and e-mails, patient in staying with me in the laboratory, despite being also writing her doctoral thesis and wish her all the luck for her thesis defense.

Then I would like to thank to all the people of the laboratory "E3.P2.019" situated in the Faculty of Pharmacy, that somehow helped me in my work, especially to Dr. Cláudia Nunes for all the doubts answered and willingness contagious; to MSc Catarina Alves for all the good advices and aid given; to MSc Ana Rute Neves for all the sympathy and readiness in schedule my appointements in DLS; to my colleagues Catarina Moura and Miriam Machado who helped me in my experiences. Thank you all for providing a great work environment along these months.

I would like to thank my family, for all the patient, understanding and support granted along these five years.

I would also like to thank to my boyfriend for all the patient, company and support.

Finally I would like to thank to all the people who made this five years so special in the Faculty of Engineering, my fellow colleagues, my dear girls from Tuna Feminina

de Engenharia (TUNAFE) and my closest friends for all the motivation, company, support to overcome all the difficulties, good moments and “suffering” shared in all the exams, sleepless nights and finally in concretize this goal, finishing my course.

To all of you, my sincere Thanks.

ABSTRACT

This work focuses on the biophysical interactions of isoniazid (INH) and rifampicin (RIF), two commonly drugs used in the front-line treatment of tuberculosis (TB), with 3D membrane models. Liposomes made of dipalmitoylphosphatidylcholine (DPPC) were used to mimic the human membranes, at the physiologic pH. In this study, INH's and RIF's membrane partition were evaluated, their preferential location within the membrane, and their effect on the biophysical properties of the membrane, which are believed to be related with the antimycobacterial compounds mechanisms of action.

The INH's and RIF's lipophilicity was quantified by the partition coefficient (K_p) using derivative spectrophotometry. To predict the drug's location across the membrane, fluorescence quenching studies were performed using liposomes labeled with two different fluorescence probes. To evaluate the effect of INH and RIF on the membrane's biophysical properties, dynamic light scattering (DLS) was performed.

The RIF's and INH's partition results revealed that both drugs establish, respectively, electrostatic and hydrogen bonds with the phospholipids head groups. Fluorescence quenching measurements allowed concluding that INH might be located at the surface of the membrane or deeply buried in the bilayer, reaching the aqueous vacuole. RIF initially interact with the phospholipids head groups, and then adopts a deeper position in the hydrocarbon core of the bilayer. Moreover, the changes in the biophysical parameters are in agreement with the abovementioned. Therefore this study may contribute to the discovery of novel drugs for TB chemotherapy.

Keywords: Biophysical interactions, Dynamic light scattering, Fluorescence quenching, Liposomes, Partition coefficient, Tuberculosis.

RESUMO

Este trabalho focou-se nas interações biofísicas da isoniazida (INH) e da rifampicina (RIF), dois fármacos geralmente utilizados no tratamento de primeira linha da tuberculose (TB), com modelos membranares 3D. Foram usados lipossomas constituídos por dipalmitoilfosfatidilcolina para mimetizar as membranas humanas a pH fisiológico. Assim, com estes modelos membranares foram avaliados parâmetros como a partição da INH e da RIF na membrana, as suas localizações preferenciais dentro desta e os seus efeitos nas propriedades biofísicas da membrana, que se acredita estarem relacionadas com os mecanismos de ação dos compostos antimicobacterianos.

A lipofilicidade da INH e da RIF foi quantificada através do coeficiente de partição (K_p) através da espectrofotometria derivativa. Para prever a localização dos fármacos ao longo da membrana foram executados estudos de desativação de fluorescência, usando lipossomas marcados com duas sondas fluorescentes diferentes. Para avaliar o efeito da INH e da RIF nas propriedades biofísicas da membrana, foi realizada a técnica de "dynamic light scattering" (DLS).

Os resultados da partição da RIF e da INH revelaram que os dois fármacos estabelecem, respetivamente, ligações eletrostáticas e de hidrogénio com as cabeças dos fosfolípidos. As medições de desativação de fluorescência permitiram concluir que a INH se deverá localizar a nível da superfície membranar ou profundamente inserida na bicamada, alcançando o vacúolo aquoso. A RIF inicialmente interage com a cabeça dos fosfolípidos, e depois adota uma posição mais profunda a nível da bicamada lípidica e junto às caudas hidrofóbicas. As alterações nos parâmetros biofísicos estão também de acordo com os resultados obtidos. Assim, este trabalho pode contribuir para a descoberta de novos fármacos para o tratamento da TB.

Palavras-chave: Coeficiente de partição, Desativação de fluorescência, Dynamic light scattering, Interações biofísicas, Lipossomas, Tuberculose.

CONTENTS

ACKNOWLEGMENTS ..... **VII**

ABSTRACT ..... **IX**

RESUMO ..... **XI**

CONTENTS ..... **XIII**

LIST OF FIGURES ..... **XV**

LIST OF TABLES ..... **XIX**

ABBREVIATIONS AND SYMBOLS ..... **XXI**

CHAPTER 1 ..... **1**

Introduction 1

CHAPTER 2 ..... **3**

Context 3

2.1 Tuberculosis 3

2.1.1 Epidemiology 3

2.1.2 Pathophysiology 6

2.1.2.1 Tuberculosis types 6

2.1.2.2 Microbiology of *Mycobacterium tuberculosis* 7

2.1.2.3 Host-pathogen interactions 8

2.1.3 Tuberculosis Treatment 9

2.2 Isoniazid 11

2.2.1 Mechanism of Action of Isoniazid 12
2.3 Rifampicin 13
2.3.1 Mechanism of Action of Rifampicin 14
2.4 Biological Membranes 15
2.4.1 Membrane Models 15
2.4.2 Liposomes 16
2.4.2.1 Liposomes Classification 16
2.4.2.2 Liposomes Preparation 17
2.4.2.3 Dipalmitoylphosphatidylcholine 18

CHAPTER 3 20

Materials and Methods 20
3.1 Reagents 20
3.2 Preparation of liposomes 20
3.3 Determination of INH's and RIF's partition coefficients by derivative spectrophotometry 21
3.4 Membrane location studies by fluorescence quenching 21
3.5 Membrane biophysical properties studies 22

CHAPTER 4 23

Results and Discussion 23
4.1 Drug's membrane partition 23
4.2 Drug's membrane location 27
4.3 Biophysical modifications of the membrane 30

CHAPTER 5 33

The conclusions 33

Future perspectives 35

REFERENCES 36

LIST OF FIGURES

FIGURE 1 **TB incidence and prevalence rates in 2011.** Estimated TB incidence rates (A). Estimated HIV prevalence in new TB cases (B). Reproduced from Global Tuberculosis Report [14]. 4

FIGURE 2 **Global trends of TB incidence, prevalence and mortality.** Global trends in estimated rates of TB incidence, prevalence and mortality. Left: HIV-positive TB (green) and estimated incidence rate of HIV-positive TB (red). The horizontal dashed lines represent the targets of a 50% reduction in prevalence and mortality rates by 2015 compared with 1990. Shaded areas represent uncertainty bands. Mortality excludes TB deaths among HIV-positive people (A). Estimated absolute numbers of TB cases and deaths (in millions) (B). Reproduced from Global Tuberculosis Report [14]. 5

FIGURE 3 **Stages of granuloma formation in TB.** Initially occurs the expansion of the bacterial population in the absence of adaptive immunity. Later initiation of adaptive immunity occurs, $CD4^+$ and $CD8^+$ effector T lymphocytes are recruited to infected tissue and curtail bacterial growth. Finally, the mature granuloma represents the equilibrium between virulent mycobacteria and the host immune response. Data collected from [16]. 9

FIGURE 4 **Clinical problems of current TB chemotherapy treatment.** Data collected from [30]. 10

FIGURE 5 **Chemical structure of INH.** 11

FIGURE 6 **Chemical structure of RIF.** 13

FIGURE 7 **Liposomes classification regarding their size and number of lipid bilayers.** MLVs: Multilamellar vesicles; ULVs: Unilamellar vesicles; SUVs: Small lamellar vesicles; LUVs: Large lamellar vesicles. Data collected form [30]..... 17

FIGURE 8 **MLVs and LUVs preparation.** (1) Addition of the aqueous buffer to the phospholipid film; (2) Vortexing releases the lipid film from the flask walls; (3) The phospholipids aggregate into large liposomes with multiple bilayers – MLVs; (4) A population with a relatively narrow homogeneous size distribution constituted by one single bilayer – LUVS can be prepared by extrusion of liposomes through polycarbonate filters with well defined porous [30]. 18

FIGURE 9 **Chemical structure of DPPC.**..... 19

FIGURE 10 **Absorption spectra (A), second (B) and third (C) derivative spectra of INH (150 µM) incubated in DPPC liposomes (orange lines) and DPPC without drug (black lines) with different concentrations (M): (1) 0, (2) 5 × 10^{-5}, (3) 1 × 10^{-4}, (4) 2 × 10^{-4}, (5) 3 × 10^{-4}, (6) 4 × 10^{-4}, (7) 5 × 10^{-4}, (8) 6 × 10^{-4}, (9) 7 × 10^{-4}, (10) 9 × 10^{-4}, (10) 1 × 10^{-3}. The curve (D) represents the best fit by Eq. (1) using a nonlinear least-squares regression method at wavelength 304 nm where the scattering is eliminated.** 25

FIGURE 11 **Absorption spectra (A) and second (B) derivative spectra of RIF (30 µM) incubated in DPPC liposomes (orange lines) and DPPC without drug (black lines) with different concentrations (M): (1) 0, (2) 5 × 10^{-5}, (3) 1 × 10^{-4}, (4) 2 × 10^{-4}, (5) 3 × 10^{-4}, (6) 4 × 10^{-4}, (7) 5 × 10^{-4}, (8) 6 × 10^{-4}, (9) 7 × 10^{-4}, (10) 9 × 10^{-4}, (10) 1 × 10^{-3}. The curve (C) represents the best fit by Eq. (1) using a nonlinear least-squares regression method at wavelength 363 nm where the scattering is eliminated.**..... 26

FIGURE 12 **Stern-Volmer plots of the probe DPH (o) and TMA-DPH (•) in DPPC liposomes (500 µM, *T* = 60 ºC pH 7.4) by increasing concentrations (M) of the quencher RIF.**..... 29

FIGURE 13 **Count rate plots in absence (■) and presence (•) of INH (30 μM) (A) and RIF (30 μM) (B) in DPPC liposomes at pH = 7.4 as a function of temperature.**.....30

LIST OF TABLES

TABLE 1 **Pathogenesis and distribution of different TB cases.** Distribution of TB cases in HIV- negative patients (brown) and in HIV-positive patients (black). PTB, pulmonary tuberculosis; LNTB, lymph node tuberculosis; GUTB, genitourinary tuberculosis; MTB, military tuberculosis; TBM, tuberculosis meningitis; ABD, abdominal tuberculosis. Data collected from[20-22]. 7

TABLE 2 **Partition coefficients (K_p in M^{-1} and Log$D$ dimensionless) for DPPC liposomes (500 µM, T = 60ºC pH 7.4), at the fluid phase.** 26

TABLE 3 **Values of Stern-Volmer constant (K_{SV}) at T = 60 ºC obtained for RIF in DPPC liposomes (500 µM, T = 60 ºC pH 7.4) labeled with DPH and TMA-DPH probes.** 29

TABLE 4 **Values of main phase transition temperature (T_m) and cooperativity (B) obtained for DPPC liposomes (500 µM, T = 60.0 °C pH 7.4) in the absence and in the presence of INH or RIF (30 µM).** 31

ABBREVIATIONS AND SYMBOLS

Lists of abbreviations

ABD	Abdominal Tuberculosis
AIDS	Acquired Immunodeficiency Syndrome
DLS	Dynamic Light Scattering
DMPC	Dimyristoylglycerophosphocholine
DMPG	Dimyristoylglycerophosphoglycerol
DNA	Acid Deoxyribonucleic
DPH	1,6-diphenyl-1,3,5-hexatriene
DPPC	Dipalmitoylphosphatidylcholine
DSC	Differential Scanning Calorimetry
EMB	Ethambutol
GUTB	Genitourinary Tuberculosis
HIV	Human Immunodeficiency Virus
IFN	Interferon
INH	Isoniazid
L_α	Liquid-Crystalline Phase
L_β	Gel Phase
L_c	Sub gel Phase
LNTB	Lymph Node Tuberculosis
LUVs	Large Unilamellar Vesicles
MDR	Multi-drug Resistance
MLVs	Multilamellar Vesicles
MTb	*Mycobacterium tuberculosis*

MTB	Military Tuberculosis
$P_{\beta'}$	Ripple Phase
PC	Phosphatidylcholines
PTB	Pulmonary Tuberculosis
PZA	Pyrazinamide
TB	Tuberculosis
RIF	Rifampicin
RNA	Acid Ribonucleic
SLBs	Supported Lipid Bilayers
SUVs	Small Unilamellar Vesicles
TBM	Tuberculosis Meningitis
TMA-DPH	1-(4-trimethylammonium)-6-phenyl-1,3,5-hexatriene
ULVs	Unilamellar Vesicles
XDR	Extensively Drug Resistance
WHO	World Health Organization

List of symbols

D_T	Absorbance value of the total amount of drug
pK_a	Acid dissociation constant
r_s	Average count rate
B	Cooperativity
$[Q]_m$	Concentration of the quencher partitioned in the membrane
r_s	Count rate
$LogD$	Logarithm of the distribution coefficient
D_m	Drug distributed on the lipid membrane phase
D_w	Drug distributed in the aqueous phase
I_0	Fluorescence intensity in the absence of the quencher
I	Fluorescence intensity in the presence of the quencher
I	Ionic strength
$[L]$	Lipid concentration
V_m	Lipid molar volume
$LogP$	Logarithm of the partition coefficient
K_p	Partition coefficient
T_m	Main phase transition temperature
M	Molar
D	Second or third derivative intensity
K_{sv}	Stern-Volmer constant
T	Temperature
$[Q]_T$	Total drug concentration
α_m	Volume fraction of the membrane phase
V_T	Volume of the water phase
λ	Wavelength

CHAPTER 1

INTRODUCTION

Tuberculosis (TB) is an infectious disease and, among the communicable diseases, is the second leading cause of illness and death worldwide after HIV/AIDS (human immunodeficiency virus/acquired immunodeficiency syndrome). It is estimated that one-third of the world's population is infected with the etiologic agent of TB. TB is caused by the pathogen *Mycobacterium tuberculosis* (MTb), which has a unique cell wall, mostly made up from mycolic acids. This tubercle bacillus has the ability to penetrate the host phagocytic cells and there survive, multiply and interfere with the phagosome maturation pathway [1-3].

Isoniazid (INH) and rifampicin (RIF) are front line drugs used in the treatment of TB. INH is a prodrug, and its activity, as anti-TB drug, requires its activation. Once activated, INH has a number of target functions, including inhibition of mycolic acids synthesis causing disturbances on the replication of the bacterium [4-6]. Despite the above mentioned, the mechanism of activation of this prodrug remains poorly understood and its mechanism of action is not fully established. RIF acts via the inhibition of deoxyribonucleic (DNA)-dependent ribonucleic (RNA) polymerase, leading to a suppression of RNA synthesis, protein synthesis and consequently cell death [7].

To achieve the purpose of this work, liposomes were used as membrane models of the human membranes. Liposomes are widely chosen in many studies to understand drug-membrane interactions. They possess an ordered molecular arrangement and

they can account the electrostatic forces, which make them excellent models to predict the interaction of drugs with the biological membranes [8,9].

Dipalmitoylphosphatidylcholine (DPPC) was chosen, in this work, to formulate the liposomes, since it makes up to about one-third of total phospholipids present in the biologic membranes [10]. All the experiments were performed at the physiologic pH (i.e., pH = 7.4).

The aim of this project is to study the interactions of INH and RIF, two anti-TB drugs, with 3D membrane models namely liposomes, with the purpose to analyse the membrane partition of the drugs, understand how they penetrate into the membrane, what are the membrane biophysical consequences of the drugs, and their preferential location within the lipid bilayer. These properties can be related to their mechanism of action, namely, their entrance into the cellular compartments and toxic effects and be helpful to identify novel biophysical mechanisms capable to explain the therapeutic effects of these antimycobacterial compounds, hence allowing the future development of more effective drugs.

The work will then be divided in three major parts. The first will consist in the determination of the liposome/water partition coefficient, (K_p) to measure the drug's lipophilicity using derivative spectrophotometry. Comparing with the octanol/water, this method allows a better description of the drugs distribution between aqueous and membrane phases, and a more reliable characterization of the drug interactions with the biological membranes. Derivative spectrophotometry will be used to determine K_p, in order to eliminate the light scattering caused by the lipid vesicles [9,11,12]. Dynamic light scattering (DLS) will be used to understand the influence of the drugs on the biophysical parameters of the membrane, such as cooperativity and the main phase transition temperature (T_m). The last part will be dedicated to the determination of the drugs location within the lipid bilayer by fluorescence quenching studies. Two probes, with constant fluorescence, will be used with a well-known and different location within the lipid bilayer. The quenching constant, called Stern-Volmer constant (K_{sv}) is an indirect measure of the drug's preferential location in the membranes. Therefore, a higher K_{sv} obtained indicates a greater proximity of the quencher (i.e. drug) to the probe [13].

CHAPTER 2

CONTEXT

2.1 Tuberculosis

The history of tuberculosis (TB) mixtures with the history of humanity since TB is one of the oldest infectious diseases affecting mankind.

In the past two decades, TB has gone from being a forgotten disease to a modern and recrudescent pathology, triggered by emergence of acquired immunodeficiency syndrome (AIDS) and an increase in homelessness and poverty in the developed world. The identification of multi-drug resistance (MDR) strains and extensively drug resistance (XDR) strains has worsened this public health concern.

New effective drugs, better vaccines, and new diagnostic methods are desperately needed to change and overcome this situation.

2.1.1 Epidemiology

Currently TB ranks as the second leading cause of death from infectious disease worldwide, after the human immunodeficiency virus (HIV). According to the World Health Organization (WHO), in 2011, 8.7 million new cases of TB were estimated, which is equivalent to 125 cases per 100 000 population. Most cases where found in Asia (59%) and Africa (26%), with smaller proportions in the Eastern Mediterranean

Region (7.7%), the European Region (4.3%) and the Region of the Americas (3%) (FIGURE 1).

The five countries that rank first to fifth in the world in terms of total numbers of incident cases in 2011 were India, China, South Africa, Indonesia and Pakistan. Of 8.7 million incident cases, an estimated 0.5 million were children and 2.9 million occurred among women. About 13% of the worldwide TB caseload was HIV-associated and most of these cases were in the African Region [14].

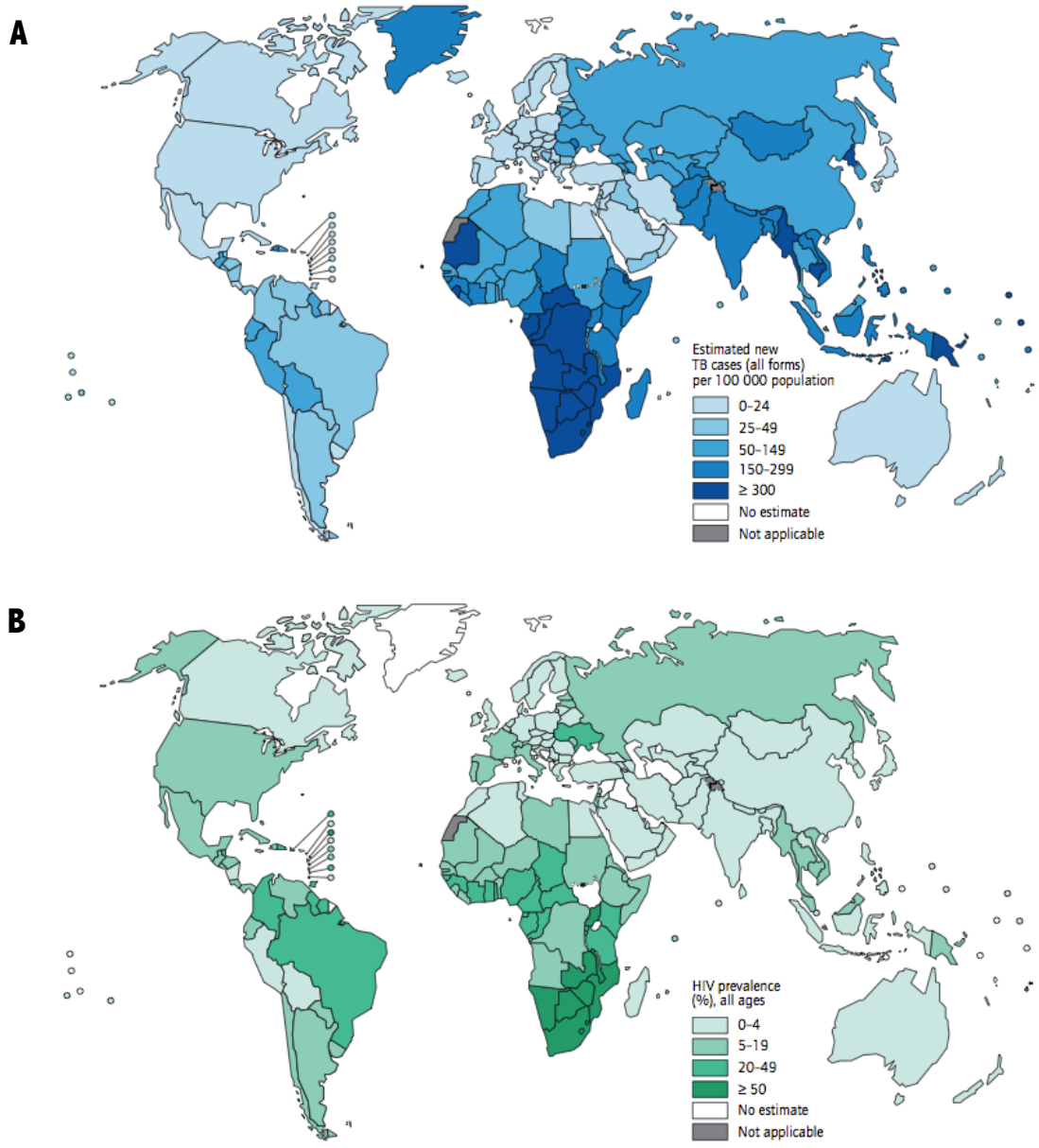

FIGURE 1 **TB incidence and prevalence rates in 2011.** Estimated TB incidence rates (A). Estimated HIV prevalence in new TB cases (B). Reproduced from Global Tuberculosis Report [14].

In 2011, TB killed approximately 1.4 million people worldwide, of whom 430 000 were HIV-positive and the other 990 000 HIV-negative. These deaths included 0.5 million among women, making TB one of the top killers of women worldwide.

In FIGURE 2 is possible to observe that, globally, incidence rates are declining. Therefore, from 1990 up to around 2011 the incidence rates were relatively slow, and then started to fall. If this trend is sustained global targets for TB control set for 2015 will be achieved: incidence should be falling and the prevalence and death rates should be halved compared to 1990.

In addition, people who are latently infected constitute the hidden reservoir of the disease from which new cases of active TB can emerge.

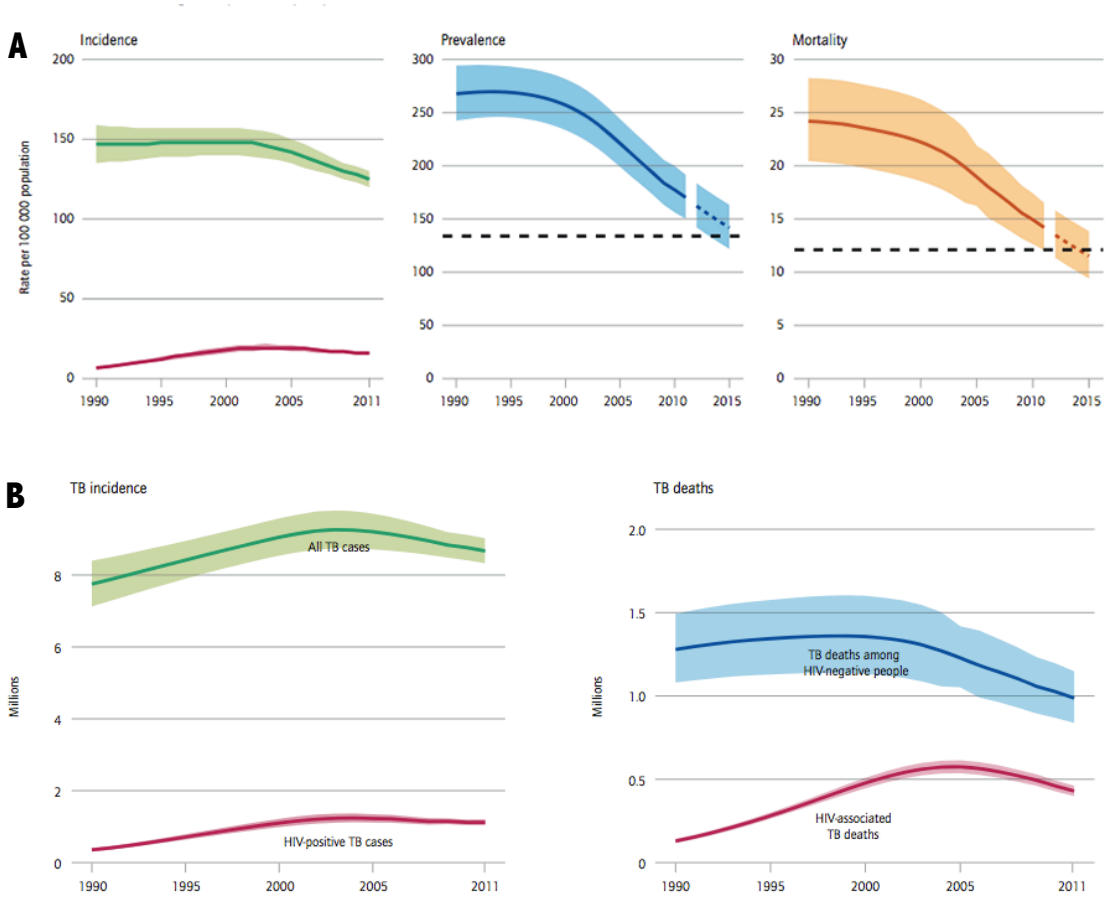

FIGURE 2 **Global trends of TB incidence, prevalence and mortality.** Left: Global trends in estimated rates of TB incidence including HIV-positive TB (green) and estimated incidence rate of HIV-positive TB (red). The horizontal dashed lines represent the targets of a 50% reduction in prevalence and mortality rates by 2015 compared with 1990. Shaded areas represent uncertainty bands. Mortality excludes TB deaths among HIV-positive people (A). Estimated absolute numbers of TB cases and deaths (in millions) (B). Reproduced from Global Tuberculosis Report [14].

2.1.2 Pathophysiology

TB is an airborne disease initiated by the inhalation of droplets (aerosols) containing a small number of the bacilli *Mycobacterium tuberculosis* (MTb) [15]. The bacilli diffuse from the site of initial infection, in the lung, through the lymphatic and blood to other parts of the body. The contamination is spread through the air when sick people with pulmonary TB expel bacteria, for example by coughing [16].

Once in the lung, one of the first interactions between MTb and the host is with the innate immune system, more specifically the resident macrophages (i.e., alveolar macrophages) responsible for the phagocytosis mediated by various host receptors. Most immunocompetent individuals either eliminate MTb or contain it in a latent state. According to appropriate stimuli, alveolar macrophages activate, and response effectively by transferring the phagocytized MTb to the destructive environment of lysosomes. Although some bacilli are able to escape lysosomes digestion, survive and multiply within the macrophage creating a dynamic balance between bacterial persistence and host defense develops [16-18]. This balance might be lifelong, since only a minority (approximately 10%) develops active clinical disease. In fact in most healthy individuals, the immune defense system retains sufficient control over replication of the bacterium such that the individual remains free of tissue damage and symptoms, in a so-called state of latency [19].

2.1.2.1 Tuberculosis types

Although TB can affect any organ, the pulmonary TB is the most common manifestation of the disease, being the lung the main organ affected by the disease. Extrapulmonary TB has been used to describe the infection at body sites other than the lung, as for example, in the liver, kidney, spine, brain, etc. In addition, extrapulmonary TB may coexist with pulmonary TB as well. Symptoms and signs can be specific of the disease or non-specific, such as fever, weight loss, and night sweats. TABLE 1 represents the pathogenesis of different TB cases and their distribution [20-22].

TABLE 1 **Pathogenesis and distribution of different TB cases.** Distribution of TB cases in HIV-negative patients (brown) and in HIV-positive patients (black). PTB, pulmonary tuberculosis; LNTB, lymph node tuberculosis; GUTB, genitourinary tuberculosis; MTB, military tuberculosis; TBM, tuberculosis meningitis; ABD, abdominal tuberculosis. Data collected from[20-22].

Case		Pathogenesis	Distribution		
PTB		Lung's infection.	75% 30%		
EPTB	LNTB	Local manifestation of a systemic disease. MTb undergoes haematogenous and lymphatic dissemination. Cervical adenopathy is the most common.	35%	15% 20%	Both 5% 50%
	Pleural TB	Rupture of a diseased area into the pleural space.	20%		
	Bone and Joints TB	Commonly affects the thoracic spine and hip joint.	10%		
	GUTB	Renal disease may be the result of direct infection of the kidney and lower urinary tract or may present as secondary amyloidosis.	9%		
	MTB	Any progressive, disseminated form of TB.	8%		
	TBM	Neurological TB with intense inflammation following rupture of a subependymal tubercle into the subarachnoid space.	5%		
	ABD	Encompass TB of the gastrointestinal tract, peritoneum, omentum, mesentery and its nodes and other solid intra-abdominal organs such as liver, spleen and pancreas.	3%		
	Others	For example: tuberculous pericarditis, and TB associated with tumor necrosis factor-α (TNF-α) inhibitors.	10%		

2.1.2.2 Microbiology of *Mycobacterium tuberculosis*

The German physician, Robert Koch, first discovered MTb in 1882. This pathogenic bacillus is an obligate aerobe rod-shaped, acid-fast, non-encapsulated, non-spore forming and non-motile. It grows most successfully in organs with a high oxygen content, such as the lungs [23,24]. The unusual and robust MTb cell envelope is lipid-rich, composed of mycolic acids, and conferring capacity to the bacteria to survive in the host environment and resist to drug therapy. The cell wall composition is also responsible for the impermeability to basic bacteriological dyes, thus MTb is neither Gram-positive nor Gram-negative, but instead is classified as acid-fast using Ziehl-Neelsen method. The process of cell division of MTb is extremely slow, 15-20h, when compared with other bacteria, plus the ability to persist in latent state results in the need of long treatment duration of several anti-TB drugs [17,24,25].

2.1.2.3 Host-pathogen interactions

One of the first interactions between MTb and the immune system is with the macrophages and seems to be mediated by pattern recognition receptors. Cholesterol has been shown to act as a docking site for the pathogen promoting receptor-ligand interactions [18]. The precise receptor involved in the initial interaction influences the subsequent fate of MTb and the survival changes of the mycobacteria within the macrophage [17]. To persist in the host, MTb arrests the phagosome at an early stage of maturation, thereby preventing phago-lysosomal fusion and acidification of infected phagosomes. In addition, MTb also partially inhibits the activation of infected macrophages by interferon (IFN)-ϒ, residing in an environment that is only slightly acidic, with a pH of ~6.2 [1,26].

As a result, some mycobacteria persist in the lung, in a latent state, within structures termed granulomas. The granulomas (**FIGURE 3**) are structured clusters containing different types of immune cells (particularly T lymphocytes and macrophages), endothelial cells and dendritic cells, among others. This structure likely represents a balance between a potentially dangerous pathogen and the host immune system, since provides housing for MTb during a long period of time, but also prevents the spreading of the bacilli [15,17,27]. Nevertheless, the inactivation of macrophages and the arrest of phagosomal maturation are not all-or-nothing events. Some macrophages can become activated and mycobacteria phagosomes can proceed in developing to more mature stages of the phagolysosomes, acidifying to a pH of 4.5 to 5.0. It is believed that at least some proportion of the bacteria is effectively resistant to the level of acid in the phagolysosome [1].

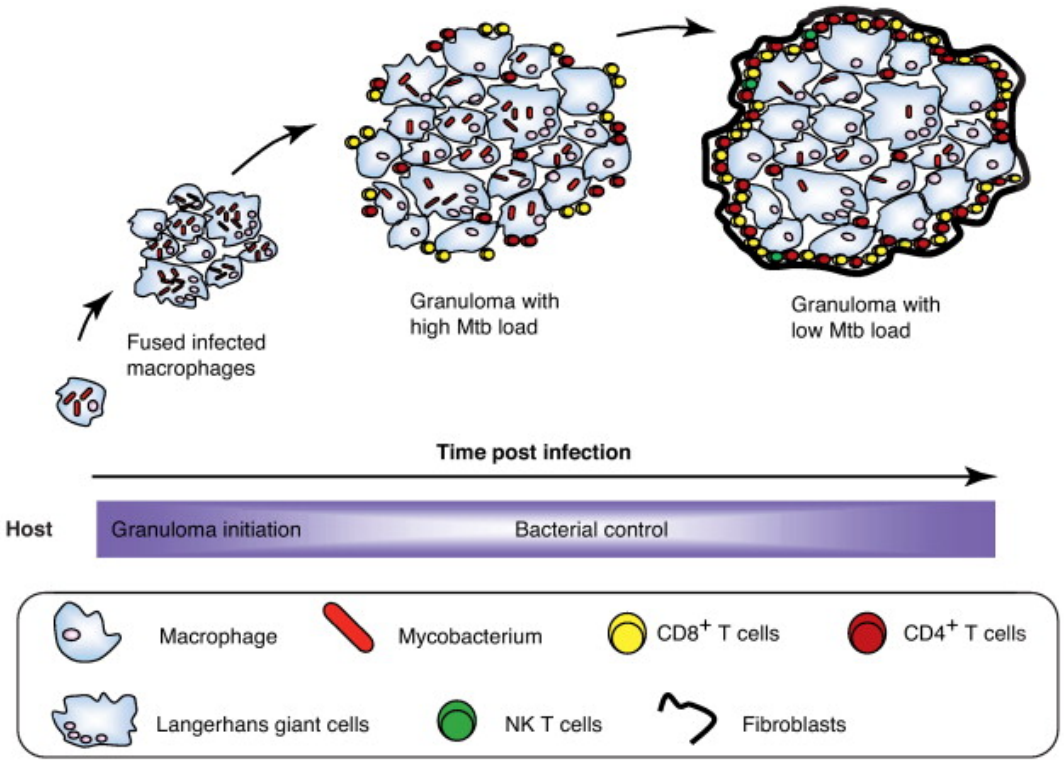

FIGURE 3 **Stages of granuloma formation in TB.** Initially occurs the expansion of the bacterial population in the absence of adaptive immunity. Later initiation of adaptive immunity occurs, $CD4^+$ and $CD8^+$ effector T lymphocytes are recruited to infected tissue and curtail bacterial growth. Finally, the mature granuloma represents the equilibrium between virulent mycobacteria and the host immune response. Data collected from [16].

2.1.3 Tuberculosis Treatment

In the past two decades, there has been the worldwide emergence of MDR, XDR and more recently strains that are resistant to all anti-TB drugs. MDR is defined as mycobacteria resistance to, at least, two anti-TB drugs, rifampicin (RIF) and isoniazid (INH), whereas XDR is defined to MDR with additional resistance to, at least, one injectable second-line anti-TB drug plus a fluoroquinolone [28]. Globally 3.7% of new cases and 20% of previously treated cases of TB were estimated to have MDR [14].

The goals of treatment include cure without subsequent relapse, prevention of death, impediment of the transmission, and prevention of the emergence of drug resistance. Currently, TB chemotherapy consists of, at least, 6-month therapy using first-line drugs [16]. Treatment of TB and drug resistance cases requires multi-drug therapy, comprising:

1) Initially, an intensive phase of RIF, INH, pyrazinamide (PZA) and ethambutol (ETB) daily for 2 months.
2) A continuation phase of RIF and INH for a further 4 months, either daily or three times per week.

If the treatment fails as a result of MDR, or intolerance to one or more drugs, second-line anti-TB drugs are used, such as para-aminosalicylate, kanamycin, rifabutin, fluoroquinolones, capreomycin, ethionamide and cycloserine, that are in general more toxic with serious side effects [29]. These current TB treatment protocols, despite highly effective, are lengthy, usually 6-9 months, which contributes to the non-patient compliance to the therapy being the cure rate unsatisfactory (FIGURE 4) [16].

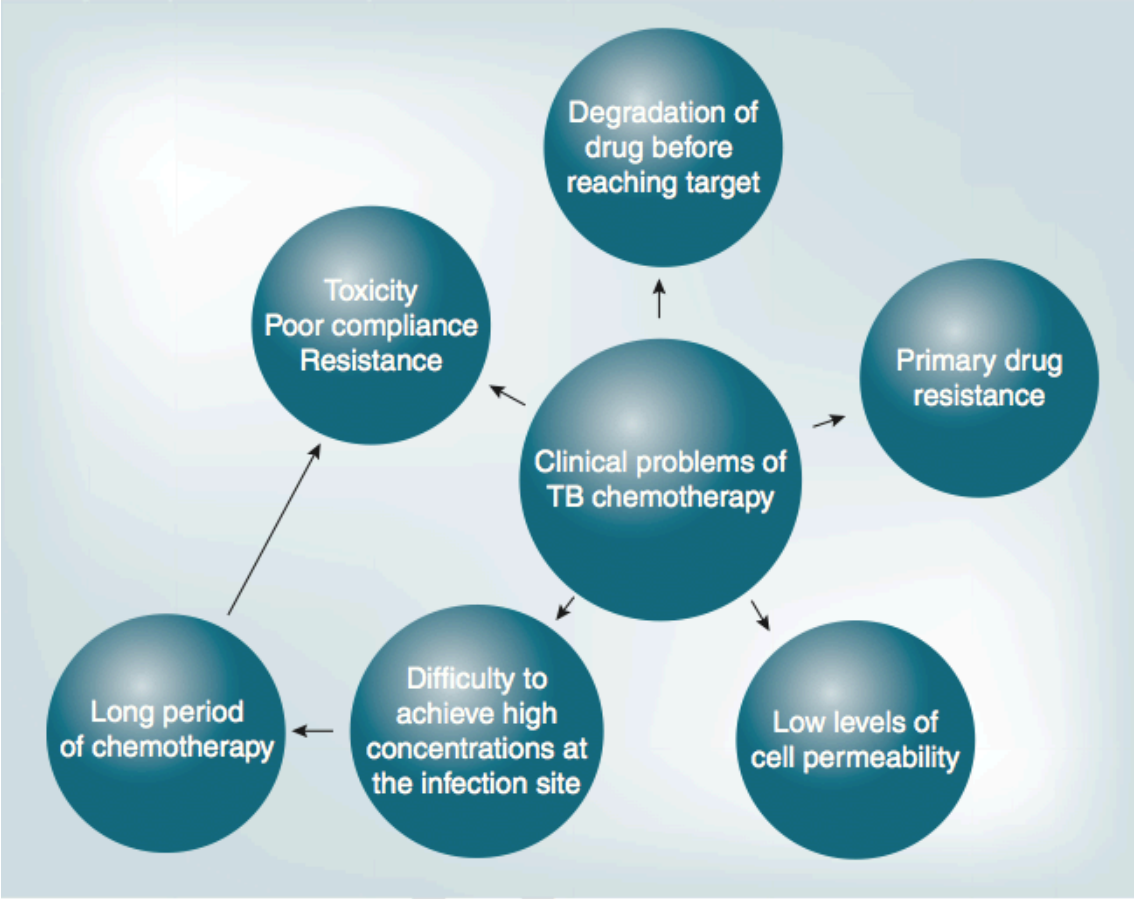

FIGURE 4 **Clinical problems of current TB chemotherapy treatment.** Data collected from [30].

2.2 Isoniazid

For more then a half a century, INH has been an essential front line drug used in TB chemotherapy, since its discovery in 1952 [31]. INH is a prodrug and requires activation before it becomes therapeutically active. Its mechanism of action seems to be related with the inhibition of the mycolic acids [4].

Chemically, INH (FIGURE 5) is a hydrazide of isonicotinic acid with three pK_a values: 1.8 for the basic pyridine nitrogen; 3.5 for the hydrazide nitrogen; 10.8 for the hydrazide group [32]. At the physiologic pH (pH = 7.4), INH is a neutral specie, since only a tiny percentage is in the ionized form (0,01%, predicted using MarvinView® 5.4.1.1 software from ChemAxon), so the interactions between the drug and the liposomes are expected to be mainly due to the hydrophobic and hydrogen bonds [8].

Following oral administration, INH is readily absorbed and does not bind to plasma proteins (plasma half-life: 1 - 1.15 h) being well distributed to different body tissues and fluids. Because of this widespread distribution, INH is an anti-TB drug effective against all types of TB [33].

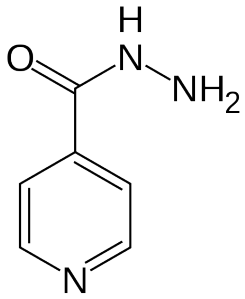

FIGURE 5 **Chemical structure of INH.**

This front line drug undergoes significant first pass hepatic metabolism, meaning that, is mainly metabolized by the liver via acetylation by the enzyme N-acetyltransferase to the inactive acetyl-INH. Since the rate of acetylation it is genetically dependent, patients can be categorized as fast acetylators (half-life: 0.5 - 1.6 h) and slow acetylators (half-life: 2 - 5 h). In slow acetylators, INH is slowly metabolized resulting into more prolonged plasma levels of the drug and possibly more adverse effects than in rapid acetylators. Acetyl-INH can be further hydrolyzed and acetylated forming the mono-acetylhydrazine that can be converted into hydrazine, which is though to be associated to hepatotoxicity of INH, a major adverse

effect [34,35]. Other side effects include dryness of mouth, epigastric distress, allergic reactions, peripheral neuritis, mental abnormalities and methaemoglobinemia.

2.2.1 Mechanism of Action of Isoniazid

INH is one of the most effective bactericidal synthetic therapeutic drug for the treatment of TB. INH enters the mycobacteria cell through passive diffusion [36]. The anti-TB function of INH requires its *in vivo* activation by the MTb catalase-peroxidase enzyme KatG. The *katG* gene encodes the former protein and mutations contribute to the loss of its function, and consequently MTb resistance to INH [31,37]. Once converted in the activated inhibitor form, INH has a number of proposed targets in the mycobacteria cell, such as the enoyl-acyl carrier protein reductase (InhA) and the β-ketoacyl acyl carrier protein synthase, leading to mycolic acid biosynthesis inhibition, long-chain fatty acid accumulation, and bacteria death [38].

The mechanism of action of INH still remains poorly understand and drug-membrane interaction studies may help to unveiling the mechanism of action of this drug.

2.3 Rifampicin

RIF is one of the most potent and broad bactericidal antibiotics and is a key drug of the anti-TB therapy. This semisynthetic drug belongs to rifamycin group and is a fermentation product of *Streptomyces mediterranei*. RIF was introduced in the market in 1968 and has greatly shortened the duration of TB chemotherapy [7,39]. The mechanism of actin of RIF is related with the inhibition of the bacterial RNA synthesis [16].

Chemically, RIF (FIGURE 6) is predominantly a zwitterion, being 40% of the molecules negatively charged at the physiologic pH, with two pK_a values: 1.7 related to 4-hydroxy and 7.9 related to 3-piperazine nitrogen [8].

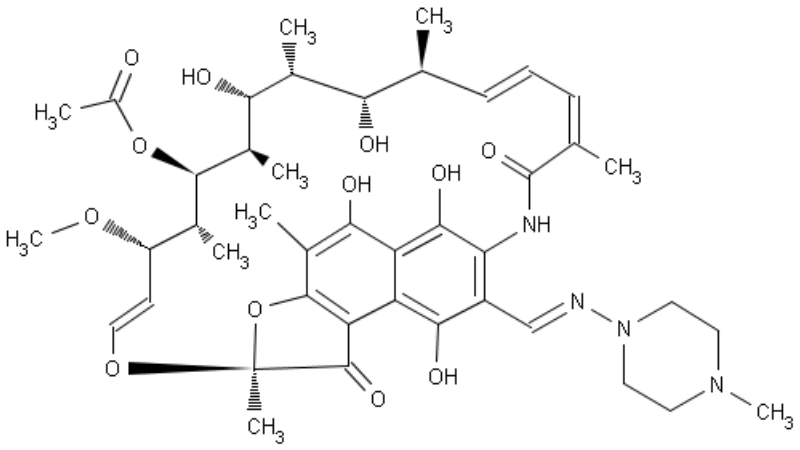

FIGURE 6 **Chemical structure of RIF.**

This anti-TB drug can be administered via oral or parental route (intravenous injection) and has higher bioavailability. Once ingested RIF is readily absorbed from the gastrointestinal tract and a large amount of drug binds to plasma proteins (half-life: 1.5 - 5 h) [39]. This front-line drug is widely distributed trough the body, diffusing freely into tissues, living cells and bacteria, making it extremely effective against intracellular pathogens like MTb [7].

The liver enzymes metabolize approximately 85% of RIF. RIF undergoes enterohepatic recirculation and is rapidly deacetylated to its main and active metabolite – desaetylrifampicin. The most serious adverse effect is related to RIF hepatotoxicity. The more common side effects include fever, gastrointestinal disturbances, rashes, discoloration of the skin and body fluids and immunological reactions [39].

2.3.1 Mechanism of Action of Rifampicin

RIF is thought to specific inhibits bacterial deoxyribonucleic acid (DNA)-dependent ribonucleic acid (RNA) chain synthesis by inhibiting bacterial DNA-dependent RNA polymerase [7,40]. This drug binds to the RNA polymerase active subunit and blocks RNA synthesis by physically preventing elongation of RNA products beyond a length of 2-3 nucleotides. However, it does not affect mammalian RNA polymerase and hence not interfere with the RNA synthesis [7,41]. Several studies provide evidence that resistance to RIF arises from mutations in *rpoB* gene, which encodes the β subunit of RNA polymerase [42].

RIF is a key component of anti-TB chemotherapy, however bacteria, such as MTb, develop resistance to this drug with high frequency restricting the utility of its use for treatment of TB or emergencies. A more detailed knowledge about the mechanism of action of RIF may be obtained by the biophysical studies of the drug-membrane interactions.

2.4 Biological Membranes

Biological membranes present a highly complex, dynamic and fluid architecture, with only a few nanometers thick, mainly composed of a lipid bilayer of water-insoluble amphiphilic compounds, particularly the phospholipids, with embedded proteins. The phospholipids are amphipathic lipids and present a hydrophilic head group facing outwards (medium) and hydrophobic tails directed towards each other [43,44]. Basic proteins, cholesterol, glycolipids and other molecules are usually inserted in biological membranes in such a way that confer the bilayer the functional properties appropriate for the particular membrane.

There are four main classes of phospholipids: phosphatidylcoline, phosphatidylethanolamine, phosphatidylserine and sphingomyelin [45]. One of the main components of eukaryotic membranes are the phosphatidylcholines (PC). PC are also critical constituents of human lung surfactant, serum lipoproteins, and bile and represent the most widely used lipid in model membrane studies [46].

Lipid bilayers present many lamellar phases as a function of temperature, namely gel phase (L_β), liquid-crystalline phase (L_α), subgel phase (L_c), and ripple phase (P_β). Above a characteristic temperature of each lipid, the main phase transition temperature (T_m), the bilayer is in a L_α phase, in which the lipid acyl chains are fluid and disordered, below that temperature the phospholipids are in an ordered L_β phase. It is widely accepted that many biologically relevant processes occur in the L_α phase, were the hydrocarbon chains are in a disordered state [47,48].

2.4.1 Membrane Models

In the past years, a considerable number of simple model membranes have been constructed in attempts to face the complexity of their biological counterparts and capture, at a molecular level, some of the essential features of drug-membrane interactions. There are many different types of membrane models, such as:

- **Micelles:** are constituted by surfactant molecules, that self-assemble in aqueous solutions at concentrations above the critical micelle concentration. This aggregate presents the hydrophilic head group in contact with the surrounding solvent, sequestering the hydrophobic single tail in the center [49];

- **Langmuir monolayers:** are a monomolecular film formed at the air-water interface [50];
- **Liposomes:** are self-closed vesicles composed of one or more lipid bilayers that encapsulate water [51];
- **Supported Lipid Bilayers (SLBs):** consists on a lipid bilayer deposited on a solid support, being the upper face the only one exposed to the solvent, providing great stability [52].

Among a variety of simplified membrane models, liposomes represent simple and reliable membrane models and therefore were used in the work to assess drug-membrane interactions [30].

2.4.2 Liposomes

Liposomes (also known as lipid vesicles) are closed spherical vesicles composed of one or more lipid bilayers. These structures are composed of amphiphilic molecules, with a hydrophilic head group and hydrophobic lipid tails, which are generally a synthetic derivative of a natural phospholipid, often dipalmitoylphosphatidylcholine (DPPC). The phospholipids spontaneously self-assemble into one or more concentric bilayers when placed in an aqueous medium, with the polar head groups in contact with the aqueous phase, and the fatty acids orientated towards each other forming the hydrophobic core shielded from the water [51,53]. Liposomes size (diameters) varies between 20 nm to several dozens micrometers, whereas the thickness of the phospholipid bilayer membrane is approximately 4-7 nm [54].

2.4.2.1 Liposomes Classification

Liposomes are commonly classified according to their size and number of lamellae (FIGURE 7). With respect to the number of bilayers it is possible to distinguish between [30]:

- **Multilamellar vesicles (MLVs):** they are a result of the thin film hydration method and are liposomes with multiple concentric bilayers within a single particle. Their size range from a few hundred to thousands of nanometers;

- **Unilamellar vesicles (ULVs):** when MLVs are sonicated or extruded, through a filter, occurs the formation of ULVs, which consist of a single membrane bilayer. Regarding their size, ULVs can be further classified into:
  - **Small Unilamellar vesicles (SUVs):** with a diameter below 100 nm;
  - **Large Unilamellar vesicles (LUVs):** with a diameter above 100 nm.

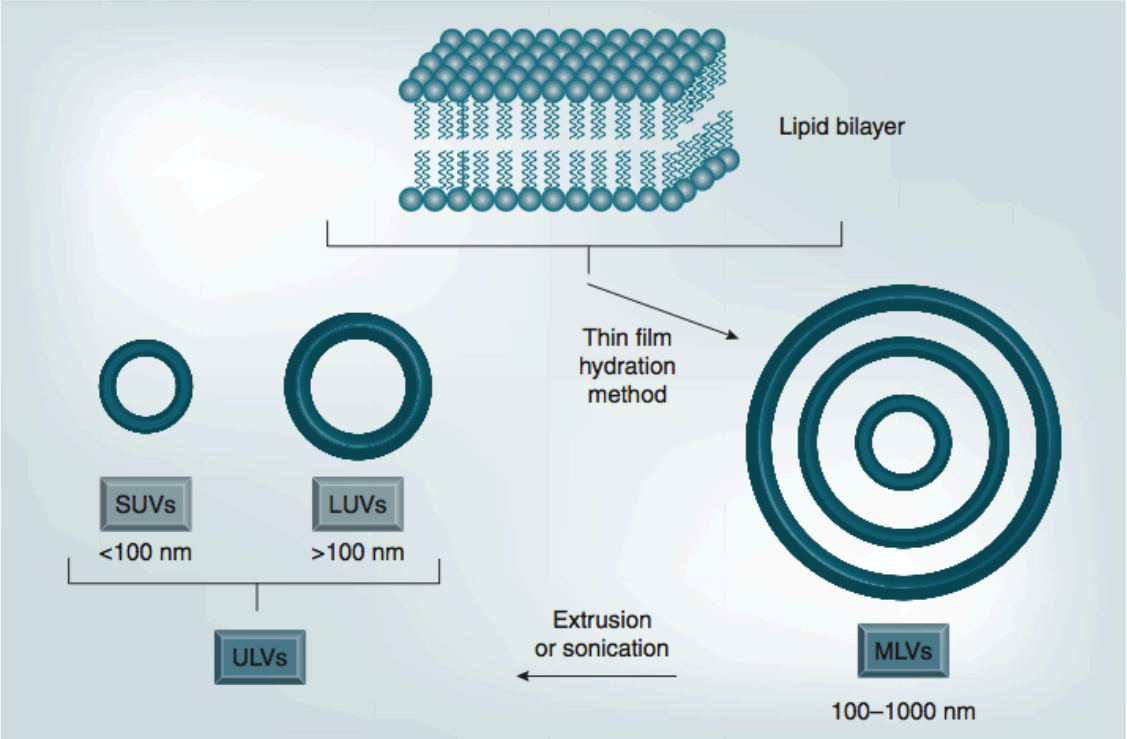

FIGURE 7 **Liposomes classification regarding their size and number of lipid bilayers.** MLVs: Multilamellar vesicles; ULVs: Unilamellar vesicles; SUVs: Small lamellar vesicles; LUVs: Large lamellar vesicles. Data collected form [30].

2.4.2.2 Liposomes Preparation

MLVs are commonly prepared by lipid hydration method. In this method, liposomes are prepared by evaporation to dryness of a lipid solution, so that a thin phospholipid film is formed. Hereafter, the film is hydrated above the T_m of the lipid, by adding aqueous buffer and vortexing the dispersion. The suspension of MLVs produced is then extruded under nitrogen through polycarbonate filters (100 nm) to form LUVs [55]. These latter liposomes were used as the membrane models in all the experimental assays in this work. All these processes are illustrated in FIGURE 8.

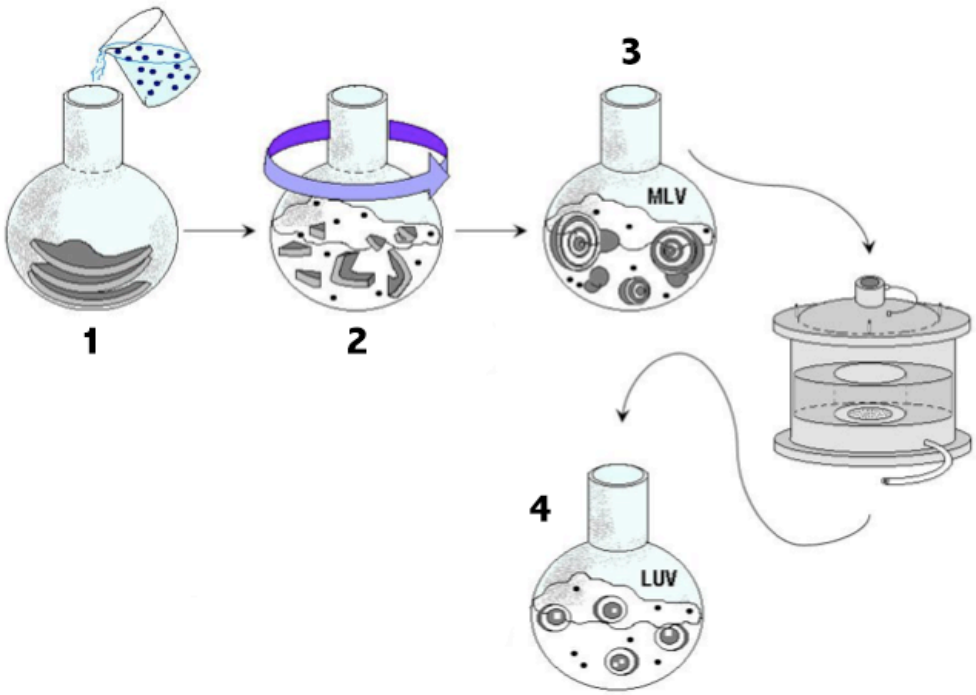

FIGURE 8 **MLVs and LUVs preparation.** (1) Addition of the aqueous buffer to the phospholipid film; (2) Vortexing releases the lipid film from the flask walls; (3) The phospholipids aggregate into large liposomes with multiple bilayers – MLVs; (4) A population with a relatively narrow homogeneous size distribution constituted by one single bilayer – LUVS can be prepared by extrusion of liposomes through polycarbonate filters with well defined porous [30].

2.4.2.3 Dipalmitoylphosphatidylcholine

Dipalmitoylphosphatidylcholine (DPPC) was chosen in this work, since it is a representative phospholipid of the biological cell membranes. DPPC is composed of a polar head, phosphatidycholine, which in turn is composed of a phosphate group (negatively charged) and a choline (positively charged). It also has in its constitution two fatty acids chains, dipalmitoyl, with 16 carbon atoms each (FIGURE 9). This fully saturated phospholipid has a transition temperature around 41 ºC and at body temperature is in the gel phase [56].

DPPC makes up to about one-third of total phospholipids presents in the body, also accounts for 10-20% of the PC content of brain myelin and erythrocyte membranes, being one of the major components of the pulmonary surfactant [10]. In pulmonary TB, the first physiological barrier encountered by the inhaled MTb is the pulmonary surfactant. The lung surfactant is a complex mixture of lipid and proteins

complex that lines the pulmonary alveoli as a surfactant monolayer at the air-aqueous interface [57,58].

According to the above-mentioned DPPC liposomes represent a suitable model to study INH and RIF interactions with the biological membranes and get a higher knowledge about its mechanism of action.

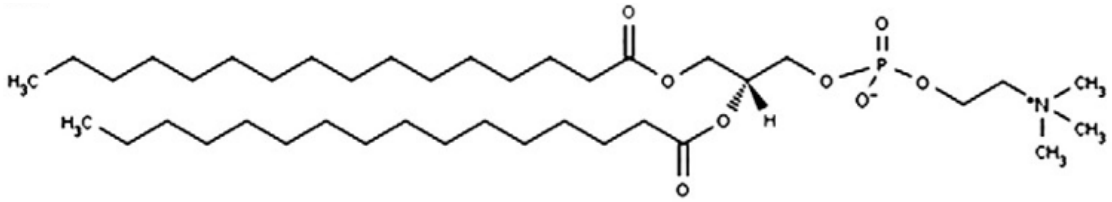

FIGURE 9 **Chemical structure of DPPC.**

CHAPTER 3

MATERIALS AND METHODS

3.1 Reagents

INH and RIF were obtained from Sigma–Aldrich Co. (St. Louis, MO, USA). DPPC was purchased from Avanti Polar Lipids (Alabaster, AL, USA). The probes 1,6-diphenyl-1,3,5-hexatriene (DPH) and 1-(4-trimethylammonium)-6-phenyl-1,3,5-hexatriene were obtained from Molecular Probes (Invitrogen, Paisley, UK). All other chemicals were purchased from Merck.

Drug solutions were prepared with phosphate buffer at pH 7.4. This buffer was prepared with double-deionized water (conductivity less than 0.1 μS cm^{-1}) from a Millipore system, and the ionic strength (I = 0.1 M) was adjusted with NaCl.

3.2 Preparation of liposomes

Liposomes were prepared according to the thin film hydration method. Concisely, the lipid, DPPC, was dissolved in a chloroform/methanol mixture. The organic solvents were then evaporated under a stream of nitrogen using a rotary evaporator to yield a dried lipid film. The resultant lipid film was hydrated with a buffer (phosphate: 0.1 M, I = 0.1 M, pH 7.4) and the mixture was vortexed to yield MLVs. Lipid suspensions were then equilibrated at 60 ºC (temperature above the main phase transition temperature) for 30 min and were further extruded one time through polycarbonate filters with a pore diameter of 600 nm, followed by one time with the

filters with a pore diameter of 200 nm and finally were extruded ten times through filters with a pore diameter of 100 nm, at 60 ºC, to form LUVs.

For DPH and TMA-DPH labeled liposomes, the probe was co-dried and with the lipid and incorporated in a ratio of 1:300 (probe:lipid).

3.3 Determination of INH's and RIF's partition coefficients by derivative spectrophotometry

The partition coefficient (K_p) of INH and RIF between LUVs suspensions of DPPC and buffer solution, at the physiologic pH, was determined by derivative spectrophotometry. Phosphate buffer solution was added to liposomes containing a fixed concentration of INH (150 μM) or RIF (30 μM) and increasing concentrations of DPPC (50, 100, 200, 300, 400, 500, 600, 700, 900, 1000 μM). The correspondent reference solutions were identically prepared in the absence of drug. All suspensions were then vortexed and incubated above the main phase transition temperature of the lipid (i.e. 60 ºC). The absorption spectra were recorded at 60 ºC by a Perkin-Elmer Lambda 45 UV-Vis spectrophotometer, using quartz cells with a 1 cm^{-1} path length and a spectral range from 250 to 550 nm at 1 nm intervals. The mathematical treatment of the results was performed using a developed routine, K_p calculator.

3.4 Membrane location studies by fluorescence quenching

The INH's and RIF's membrane location studies were assessed by steady-state fluorescence quenching measurements, using two fluorescence probes (DPH and TMA-DPH) in liposomes' buffered suspensions prepared with DPPC at pH 7.4, with a well-established and documented membrane position and depth [59,60]. The studies were carried out by incubation of drugs with the labeled liposomes. It was used a fixed concentration of DPPC (500 μM) and increasing concentrations of INH (0-150 μM) and RIF (0-100 μM). The resultant suspensions were incubated, protected from the light, for 30 min at a temperature above the main phase transition temperature of DPPC (60 ºC), allowing INH and RIF to reach the partition equilibrium between the lipid membranes and the aqueous medium. Measurements were carried out at a controlled temperature (60 ºC).

Fluorimetric data were obtained using a Jasco FP-6500 spectrofluorometer (Jasco, Great Dunmow, UK) equipped with a constant temperature cell holder. The excitation wavelength was set to 357 nm for DPH and 360 nm for TMA-DPH. The emission wavelength were set to 427 nm for DPH and 430 nm for TMA-DPH [59-61].

All fluorescence intensity data were corrected for the quencher absorbance at the excitation wavelength.

3.5 Membrane biophysical properties studies

To evaluate the effect of INH (30 μM) and RIF (30 μM) on the biophysical parameters (T_m and cooperativity) of DPPC liposomes (500 μM), a DLS technique was performed, as previously described [62].

The count rate was collected using a BI-MAS DLS instrument (Brookhaven Instruments, USA), containing a controlled temperature cell holder. The samples were heated from 30 ºC to 60 ºC with intervals of 1 ºC with an equilibration period of 2 min. At each temperature, 6 runs of 2 min were performed.

CHAPTER 4

RESULTS AND DISCUSSION

4.1 Drug's membrane partition

The drug's pharmacokinetics is greatly influenced by the lipophilicity. Drug's absorption, metabolism, binding and distribution are affected by this physicochemical factor. In general, the higher the lipophilicity of a drug, the higher its permeability, thus its absorption, the stronger its binding to protein and the greater its distribution through the body [63]. In addiction, an increment in the lipophilicity of an antimycobaterial agent positively affects the entry into the hydrophobic mycobacterial membranes and its efficacy [60].

The main predictive index of lipophilicity is a computational value, logarithm of the partition coefficient (Log*P*), which represents the octanol solubility of a given compound in the presence of aqueous solute. Generally, desirable antimycobacterial candidates should have a value for Log*P* between 1.3 and 4.1 [64]. Since INH and RIF are ionizable compounds, the partition becomes pH dependent an then, the lipophilicity is normally represented by the distribution coefficient (Log*D*).

The K_p of INH and RIF, expressed in term of Log*D*, has been determined in a liposome/buffer system using derivative transformation UV spectroscopy, since this model constitutes a more realistic prediction of drug behaviour in biological environments, in comparison with the unsatisfactory octanol/water partition method. Is also able to characterize the extent of drug penetration into the membrane and/or interactions with phospholipids or other membrane components,

mimicking better the hydrophobic part and the outer polar and negatively charged surface of the lipid bilayers [12,60,61]. Furthermore, derivative spectroscopic techniques combined with liposome/buffer system allow determining the drug distribution between the lipid and buffer media, without the need to quantify the drug separately in each media. Moreover, the intense background signals of lipid vesicles light scattering can be eliminated by the use of derivative spectrophotometry that additionally provides a better resolution of overlapped bands [59,65].

After equilibration, the absorption spectra were recorded. The partition coefficients were calculated from the second and third derivative spectra (determined from the recorded absorption spectra after blank subtraction) at the wavelength where the scattering is eliminated, by fitting Eq. (1) to the experimental data (D_T versus $[L]$) using a nonlinear least- squares regression method where the adjustable parameter is the partition constant, K_p [60,61,65]:

$$D_T = D_w + \frac{(D_m - D_w)K_p[L]V_m}{1 + K_p[L]V_m} \quad (1)$$

In this equation, D is the second or third derivative intensity ($D = (d^n\text{Abs})/(d\lambda^n)$) obtained from the absorbance values of the total amount of INH or RIF (D_T); INH or RIF distributed on the lipid membrane phase (D_m); INH or RIF distributed in the aqueous phase (D_w); lipid concentration ($[L]$); and the lipid molar volume (V_m). For DPPC, the mean molecular weight is 734.05 $gmol^{-1}$ and V_m is 0.70 $Lmol^{-1}$ [61].

In **FIGURE 10** is showed, as an example, the absorption (A), the second (B) and the third (C) derivative spectra of INH with different concentrations of LUVs of DPPC at pH 7.4 and 60 ºC. The wavelength of the maximum absorption of INH (**FIGURE 10C**) exhibits a slight decrease in the intensity with increasing DPPC concentration, providing an indication that the partition of the drug to the lipid bilayers happens [9,65]. The Kp values were obtained by fitting Eq. (1) to experimental third derivative spectra data (Dt vs. $[L]$) for 150 µM drug concentration, using a non-linear least-squares regression method at wavelength where the scattering is eliminated [61,66]. **FIGURE 10D** shows the best fit of the Eq. (1) to the third derivative spectrophotometric data collected at λ = 304 nm for INH with different concentrations of DPPC liposomes.

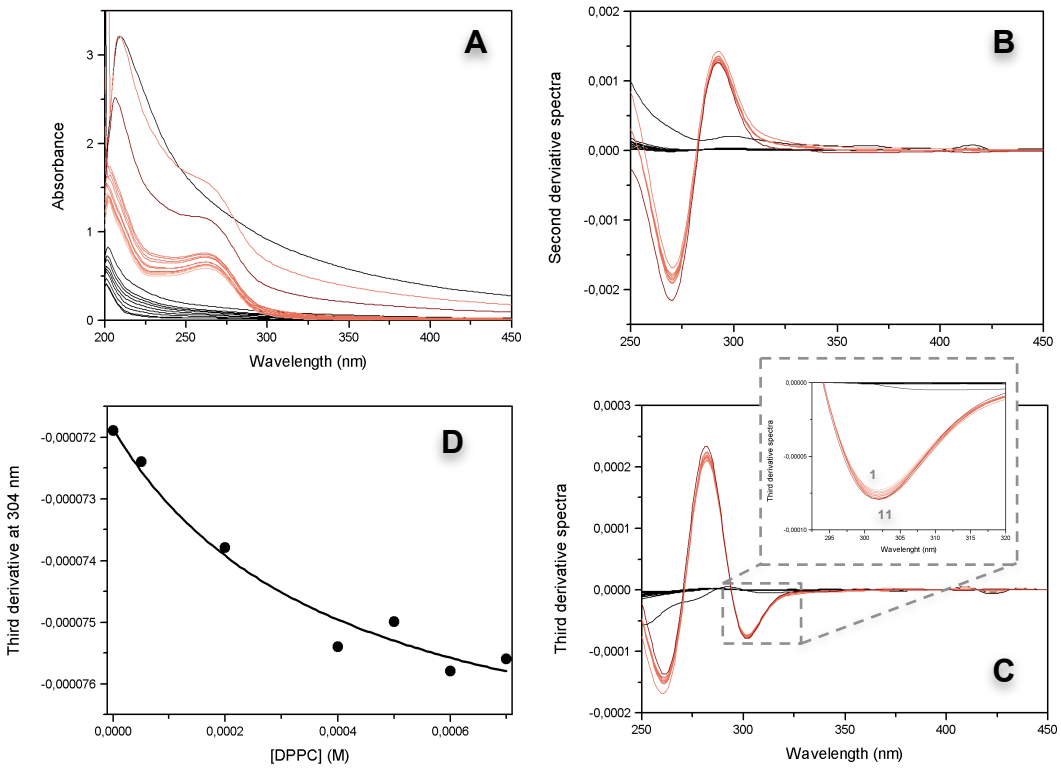

FIGURE 10 Absorption spectra (A), second (B) and third (C) derivative spectra of INH (150 μM) incubated in DPPC liposomes (orange lines) and DPPC without drug (black lines) with different concentrations (M): (1) 0, (2) 5×10^{-5}, (3) 1×10^{-4}, (4) 2×10^{-4}, (5) 3×10^{-4}, (6) 4×10^{-4}, (7) 5×10^{-4}, (8) 6×10^{-4}, (9) 7×10^{-4}, (10) 9×10^{-4}, (10) 1×10^{-3}. The curve (D) represents the best fit by Eq. (1) using a nonlinear least-squares regression method at wavelength 304 nm where the scattering is eliminated.

FIGURE 11 presents, as an example the absorption and the second derivative spectra of RIF with different concentrations of LUVs of DPPC at pH 7.4 and 60 ºC. The derivative spectra of RIF in DPPC liposomes, exhibits an increase in the intensity of the wavelength of the maximum absorption (FIGURE 11B), an observation that provides a clear indication that the drug partition happens, from the aqueous to the lipid bilayer [9,65]. The Kp values were obtained by fitting Eq. (1) to experimental second and third derivative spectra data (Dt vs. [L]) for 30 μM drug concentration, using a non-linear least-squares regression method at wavelength where the scattering is eliminated [61,66]. FIGURE 11C shows, as an example, the best fit of the Eq. (1) to the second-derivative spectrophotometric data collected at λ = 363 nm for RIF with different concentrations of DPPC liposomes.

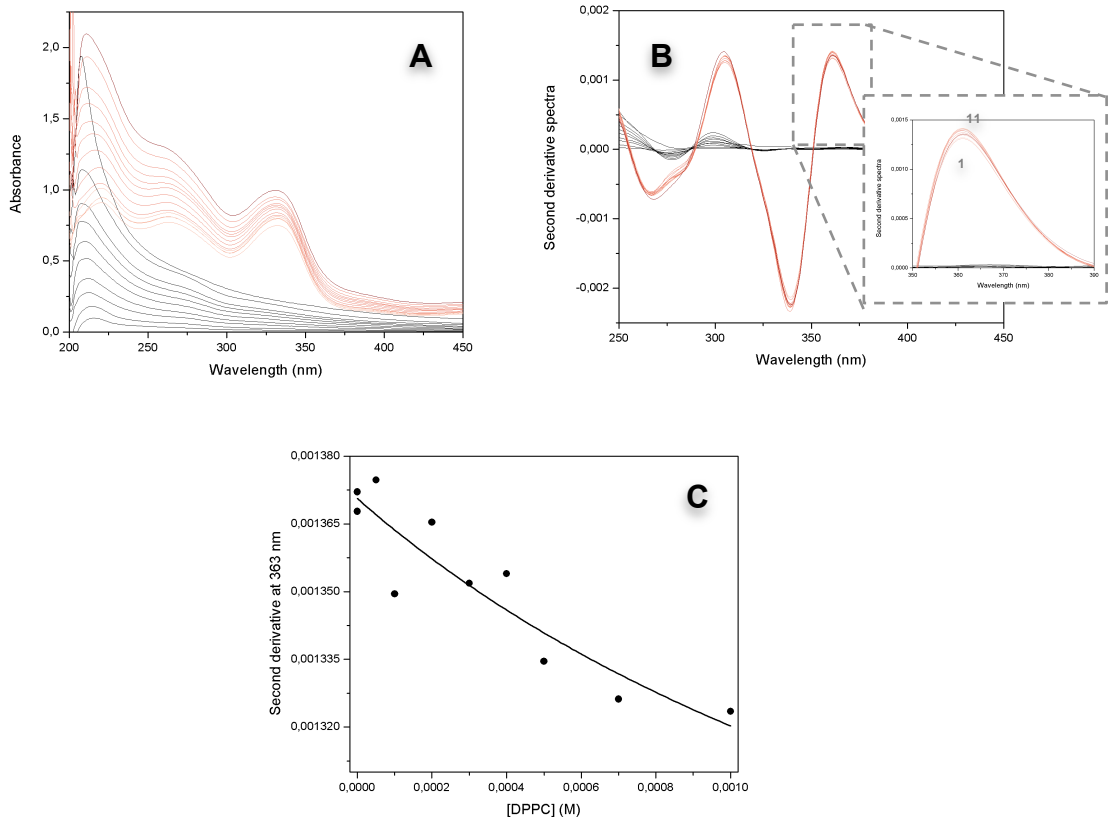

FIGURE 11 Absorption spectra (A) and second (B) derivative spectra of RIF (30 µM) incubated in DPPC liposomes (orange lines) and DPPC without drug (black lines) with different concentrations (M): (1) 0, (2) 5×10^{-5}, (3) 1×10^{-4}, (4) 2×10^{-4}, (5) 3×10^{-4}, (6) 4×10^{-4}, (7) 5×10^{-4}, (8) 6×10^{-4}, (9) 7×10^{-4}, (10) 9×10^{-4}, (10) 1×10^{-3}. The curve (C) represents the best fit by Eq. (1) using a nonlinear least-squares regression method at wavelength 363 nm where the scattering is eliminated.

TABLE 2 Partition coefficients (K_p in M^{-1} and Log*D* dimensionless) for DPPC liposomes (500 µM, *T* = 60ºC pH 7.4), at the fluid phase.

	K_p (M^{-1})	Log*D*
INH	3280 ± 729	3.7 ± 0.8
RIF	943 ± 53	3.1 ± 0.2

The Kp obtained for INH in DPPC was 3280 ± 729 and for RIF was 943 ± 53 (TABLE 2). INH molecule contains groups that can undergo protonation (pyridine, pK_a = 1.8 and hydrazide nitrogen atoms, pK_a = 3.5) and deprotonation (hydrazide group, pK_a = 10.8). According to calculations of the degree of ionization (using MarvinView® 5.4.1.1 software from ChemAxon), at physiologic pH (7.4), INH is mainly in the neutral form, with a almost negligible (0.01%) of positively charged species. The predicted Log*P*

obtained was -0.69. As expected, the predicted Log*D* was the same because INH is in the neutral form and non-charged at the physiologic pH. Though, this value is contrastingly different from the experimental Log*D* obtained, which reinforces that not only the hydrophobic forces drive the drug's partition. In fact, the ionic bonds and the hydrogen bounds also contribute to the partition with the membranes and are not or bardely accounted with the octanol/water method. In the specific case of INH, practically all the drug (99.99%) is the neutral form and therefore the ionic bonds are practically negligible [9]. Therefore, the establishment of hydrogen bonds between the drug and the polar head group of the phospholipids are probably responsible for the discrepancy of the obtained results and the predicted partition values. In fact, DPPC has in its composition much more groups that can serve as hydrogen bonds acceptors and donors in comparison with the octanol, which has only one hydroxyl group [60,67].

Regarding RIF, this molecule also has groups that can undergo protonation (hydroxyl, pK_a = 1.7) and deprotonation (piperazine nitrogen pK_a = 7.9) and at physiologic pH, this drug is manly zwitterionic with 40% of negatively charged molecules [8]. The predicted Log*P* and Log*D*, obtained using the chemical software, were, respectively, 1.39 and 0.97. The predicted Log*P* is clearly higher because it does not account the presence of charged species at the mentioned pH. As abovementioned, the significantly higher value of the experimental Log*D* compared to the calculated Log*D*, indicates that the partition of RIF with DPPC LUVs at pH 7.4 might be greatly driven by electrostatic interactions and hydrogen bonds with the polar heads of the phospholipids [60,68]. This reinforces again the idea that hydrophobic intermolecular forces are not the only interactions driving the drug's partition, which also encodes ionic bonds due to the electrostatic interactions between electrically charged species and the polar head groups of the phospholipids [60].

4.2 Drug's membrane location

Fluorescence quenching is a sensitive method that has been widely studied as a source of information about biochemical systems. The quenching of a membrane bound fluorophore provides a measure of its accessibility to the quencher (e.g. drug). Therefore, if the molecular location of a probe (fluorophore) within membranes is

well known, quenching studies can be used to reveal the location of specific ligands within liposomes and biological membranes [13].

The membrane location of INH and RIF within the lipid bilayer was assessed by steady-state fluorescence quenching measurements using two fluorescent probes (DPH and TMA-DPH). When probing the lipid membrane, the precise fluorophore location and depth in the bilayer are well established [69]. Several studies report that DPH is buried in the hydrophobic core of the membrane with a parallel alignment to the acyl chains, while TMA-DPH contains a DPH phenyl ring located within the hydrophobic acyl chains of the membrane phospholipids and a cationic group that anchors the probe in the polar head group region of the phospholipids. Therefore, TMA-DPH reports a more superficial location than DPH, nearer the phospholipid head groups [70-72].

RIF has proved to be an effective quencher of DPH and TMA-DPH, contrarily to INH that did not affected the fluorescence of the probes. The fluorescence quenching data were analyzed by the Stern-Volmer equation (Eq. (2)) [13]:

$$\frac{I_0}{I} = 1 + \mathrm{K}_{SV}[Q]_m \tag{2}$$

In this equation, I_0 and I are the fluorescence intensities in the absence and presence of the quencher, respectively; K_{SV} is the quenching constant, called Stern-Volmer constant; $[\mathrm{Q}]_m$ is the concentration of the quencher that is able to partition the membrane. This concentration was calculated from the total drug concentration ($[\mathrm{Q}]_T$) and the drug's partition coefficient (K_p), as described by Eq. (3) [13]:

$$[Q]_m = \frac{K_p[Q]_T}{K_p\alpha_m + (1 - \alpha_m)} \tag{3}$$

where α_m is the volume fraction of membrane phase ($\alpha_m = V_m/V_T$; V_m and V_T represent, respectively, the volumes of the membrane and water phases).

In FIGURE 12 is represented the Stern-Volmer plots of the probes DPH and TMA-DPH in LUVs of DPPC by increasing concentrations of RIF (I_0/I vs. $[\mathrm{Q}]_m$).

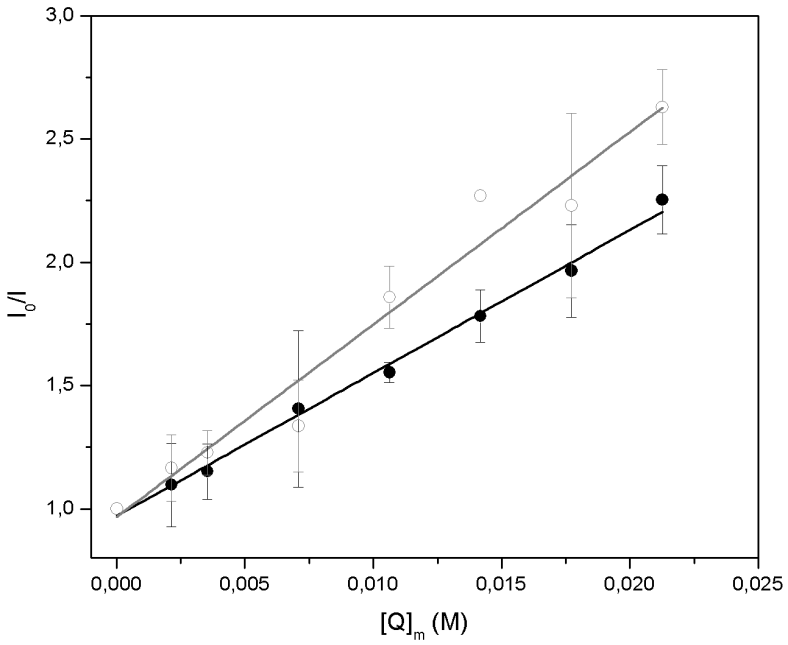

FIGURE 12 Stern-Volmer plots of the probe DPH (o) and TMA-DPH (•) in DPPC liposomes (500 µM, *T* = 60 ºC pH 7.4) by increasing concentrations (M) of the quencher RIF.

The K_{sv} values obtained for RIF in the DPPC liposomes labeled with the probes are listed in TABLE 3.

TABLE 3 Values of Stern-Volmer constant (K_{SV}) at *T* = 60 ºC obtained for RIF in DPPC liposomes (500 µM, *T* = 60 ºC pH 7.4) labeled with DPH and TMA-DPH probes.

	K_{SV} (M^{-1})
DPH	78 ± 16
TMA-DPH	58 ± 13

The location studies have shown that, the quenching of DPH and TMA-DPH is similar. These results indicate that RIF is located near both probes, being able to penetrate the lipid bilayer regarding the high values obtained for DPH. The molecules of RIF with no net charge should be inserted in the phospholipids bilayer. Moreover, the negatively charged molecules seem to be responsible for establishing electrostatic interactions with the positively charged choline present in the polar head groups of the phospholipids.

In the case of INH, the drug is not able to decreases the fluorescence intensity of both probes even at high concentrations. These results support that INH must be

located at the membrane surface completely inaccessible to both probes, or has penetrated the bilayer so deeply, maybe reaching the aqueous vacuole of liposomes.

4.3 Biophysical modifications of the membrane

The effect of INH and RIF on the lipid membrane based on the change of the biophysical parameters of DPPC liposomes was assessed by DLS studies.

FIGURE 13 presents, as an example, the results obtained with DPPC liposomes in the absence and presence of INH and RIF at pH 7.4 (FIGURE 13A) (FIGURE 13B), respectively.

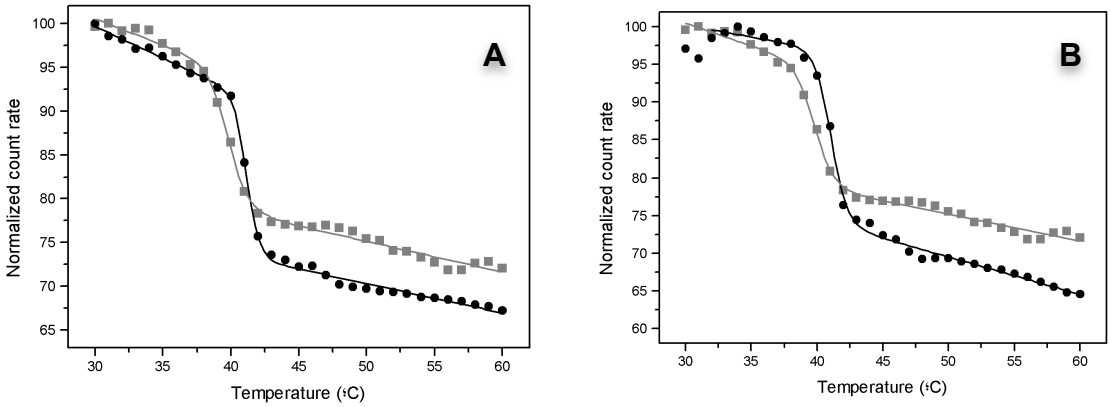

FIGURE 13 Count rate plots in absence (■) and presence (•) of INH (30 µM) (A) and RIF (30 µM) (B) in DPPC liposomes at pH = 7.4 as a function of temperature.

Using the count rate to determinate the T_m of the lipid vesicles, this technique is reliable, simple and reproducible. The mean count rate (average number of photons detected per second) versus temperature were collected and fitted using the Eq. (4) [60,62]:

$$r_s = r_{s1} + p_1 T + \frac{r_{s2} - r_{s1} + p_2 T - p_1 T}{1 + 10^{B(1/T - 1/T_m)}} \quad (4)$$

In this equation, r_s is the average count rate, T is the temperature (ºC), p_1 and p_2 correspond to the slopes of the straight lines at the beginning and at the end of the plot, r_{s1} and r_{s2} are the respective count rate intercepting values at the y axis. From the fitted data, it was possible to determine the cooperativity (B) and the midpoint of the

phase transition, which corresponds to the temperature of the gel-to-fluid transition of DPPC (T_m).

The values of cooperativity (B) and main phase transition temperature (T_m) obtained for DPPC in the presence of INH or RIF are listed in TABLE 4.

TABLE 4 Values of main phase transition temperature (T_m) and cooperativity (B) obtained for DPPC liposomes (500 µM, T = 60.0 °C pH 7.4) in the absence and in the presence of INH or RIF (30 µM).

	T_m (ºC)	Cooperativity (B)
DPPC	40.2 ± 0.6	901 ± 90
DPPC + RIF	40.8 ± 0.1	1039 ± 57
DPPC + INH	41.0 ± 0.3	1585 ± 69

The T_m and cooperativity values obtained for DPPC liposomes are consistent with previous reported studies [59,61,72].

The incorporation of INH and RIF did not affect T_m of DPPC, however in case of INH has affected significantly the lipid alkyl chain cooperativity (i.e., the number of chains that change simultaneously). Thus, INH increases the cooperativity of the phase transition in DPPC, which endorses that this anti-TB drug interacts with the lipid bilayer of the DPPC liposomes. Moreover, alterations in the biophysical parameters of the lipids give an indication about the location of the drugs within the lipid bilayers [72]. In fact, lipid bilayers are characterized by a fluidity gradient at both gel and fluid phases, i.e., the deeper region of the hydrocarbon chains near the center of the bilayer is more "fluid" and disordered (C10-C16) than the outer region of the chains near the phospholipids polar group (C1-C9) [68,73]. Therefore, biophysical parameters of the membranes, such as the cooperativity, are greatly influenced by the interaction of the drug in the C1-C9 ordered regions of the acyl chains. So, if a drug induces changes in the cooperativity and T_m is more likely to be located in the chain region near to the polar head groups (C1-C9). Contrastingly, if the drug has little or no effect in the biophysical parameters is more likely to be located in the disordered bilayer core (C10-C16) [72].

Therefore, the analysis of the changes, induced by the drugs, in the biophysical parameters of the membrane model permits to draw conclusions about the drugs location within the lipid bilayer. These results reinforce the location of INH closer to

the polar head groups of phospholipids, since this drug changes the cooperativity of the phase transition. On the other hand, RIF a bulkier molecule does not change the biophysical parameters of the lipids, possible due to a deeper penetration with the lipid bilayer in comparison with the INH.

These findings are in agreement with the abovementioned results of partition coefficient and location studies. Indeed, the interaction of INH with the membrane is essentially driven by the interactions of the drug with the polar head groups of the phospholipids via hydrogen bonds and hydrophobic forces, whereas the partition of RIF involves ionic bonds with the choline of the phospholipids head groups, possible hydrogen bonds and hydrophobic forces, specially in the case of the zwitterionic species.

CHAPTER 5

THE CONCLUSIONS

In any kind of disease, and specially in the case of TB, one of the main goals to defeat it is to find more effective and safer drugs [29].

After drug's administration, these bioactive compounds interact with many biomembranes along the body. Therefore, the study of the drug-membrane interaction, at the physiological or pathological conditions, constitutes a preliminary step to the biological (and toxic) study, as it can affect the rate of penetration of the drug in order to reach its pharmacological target, an ultimately to understand their therapeutic effects [74].

To understand how INH and RIF penetrate into the membranes, what are the membrane's biophysical consequences induced by the drugs and where their preferentially locate in the lipid bilayer, which in turn can be related with their mechanism of entrance into the cellular compartments, bioavailability and toxic effects, some biophysical techniques were performed, such as K_p, fluorescence quenching and DLS.

The overall results reveal that the partition of both drugs is high, having both drugs desirable characteristics in terms of the log*D* for an anti-TB drug. These findings also highlight how limited and unsatisfactory are the conventional models for predicting K_p, based on the octanol-water partitioning, mainly because they only account for hydrophobic interactions [66]. In fact, drugs can interact with membranes trough hydrogen bonds, which seem to be the main force responsible for the INH partitioning. The partition of the negatively charged molecules of RIF with

membranes occurs due to the ionic bonds and probably hydrogen bonds with the polar head groups of the phospholipids. The zwitterionic species, which are more hydrophobic probably, interact more deeply with the lipid bilayers. INH did not influenced the fluorescence of DPH and TMA-DPH probes, indicating that it must be located at the membrane surface completely inaccessible to both probes or has penetrated the bilayer so deeply, maybe reaching the aqueous vacuole of liposomes.

With these studies it is possible to establish important correlations with drug's therapeutic and toxic effects. In case of INH, some of the side effects include mental abnormalities, meaning that this drug passes the hematoencephalic barrier, being this probably related with the high lipophilicty described in this work for this drug. On the other hand, it is well known that DPPC lines the luminal aspects of the mucus gel layer providing the stomach with a protective layer of surface-active phospholipids, and therefore the epigastric distress caused by INH may be related with its preferential location at the head groups of the phospholipids, promoting a disruption of this protective layer [72]. Regarding to RIF, it is possible to correlate the discoloration of the skin and body fluids with RIF's high partitioning and great distribution trough the body. In a similar way described for INH the gastrointestinal disturbances may also be related with its location close to the phospholipid head groups and consequently impairment of the protective gastric layer.

Analysis of the biophysical interactions between drugs and biomembranes are becoming a settled part of the design, discovery, and characterization of new drugs candidates. Many different analytical techniques have been applied or developed on purpose to perform these kinds of studies. Using artificial membranes, as simplified models for cell membranes has given a strong input to the understanding of the complex set of interactions that a biomolecule can develop toward biological membranes.

In conclusion, the findings of this work represent a contribution to the medicinal chemistry field and permit to understand the interactions of INH an RIF with membranes, which are putatively related to the mechanism of action of these anti-TB drugs and therefore contribute to the discovery of new anti-TB drugs that effectively fight the TB.

FUTURE PERSPECTIVES

For future work, membrane models closer to biologic membranes could be used, incorporating cholesterol, glycolipids and proteins. Studies with mycolic acids that mimicks the MTb wall could also help to better understand the interactions of these drugs with the bacteria membrane.

Simulating different environment conditions, similar to those found in the infected macrophages by MTb, such as pH's of 5.0 and 6.2 could also help to understand the biophysical interactions and mechanism of action of these drugs.

Another techniques could also be used, such as differential scanning calorimetry (DSC) and steady-state anisotropy to study the influence of INH and RIF in the membrane biophysical properties. In addition, lifetime measurements could also be performed in order to understand the quenching mechanism of RIF.

REFERENCES

[1] O.H. Vandal, C.F. Nathan, S. Ehrt, Acid Resistance in Mycobacterium tuberculosis, J. Bacteriol, 191 (2009) 4714–4721.

[2] V. Deretic, R.A. Fratti, Mycobacterium tuberculosis phagosome, Mol. Microbiol, 31 (1999) 1603–1609.

[3] M.G. Gutierrez, S.S. Master, S.B. Singh, G.A. Taylor, M.I. Colombo, V. Deretic, Autophagy is a defense mechanism inhibiting BCG and Mycobacterium tuberculosis survival in infected macrophages, Cell, 119 (2004) 753–766.

[4] J. Sandy, S. Holton, E. Fullam, E. Sim, M. Noble, Binding of the anti-tubercular drug isoniazid to the arylamine N-acetyltransferase protein from Mycobacterium smegmatis, Protein Sci, 14 (2005) 775–782.

[5] C.B. Pénzes, D. Schnöller, K. Horváti, S. Bősze, Membrane affinity of antituberculotic drug conjugate using lipid monolayer containing mycolic acid, Colloid. Surface A, 413 (2012) 142–148.

[6] G.S. Timmins, V. Deretic, Mechanisms of action of isoniazid, Mol. Microbiol, 62 (2006) 1220–1227.

[7] E.A. Campbell, N. Korzheva, A. Mustaev, K. Murakami, S. Nair, A. Goldfarb, S.A. Darst, Structural mechanism for rifampicin inhibition of bacterial rna polymerase, Cell, 104 (2001) 901–912.

[8] C. Rodrigues, P. Gameiro, M. Prieto, B. de Castro, Interaction of rifampicin and isoniazid with large unilamellar liposomes: spectroscopic location studies, Biochim. Biophys. Acta, 1620 (2003) 151–159.

[9] C. Rodrigues, P. Gameiro, S. Reis, J.L.F.C. Lima, B. de Castro, Derivative spectrophotometry as a tool for the determination of drug partition coefficients in water/dimyristoyl-l-α-phosphatidylglycerol (DMPG) liposomes, Biophys. Chem, 94 (2001) 97–106.

[10] M. Mohapatra, A.K. Mishra, 1-Naphthol as a sensitive fluorescent molecular probe for monitoring the interaction of submicellar concentration of bile salt with a bilayer membrane of DPPC, a lung surfactant, J. Phys. Chem. B, 114 (2010) 14934–14940.

[11] A. Gürsoy, E. Kut, S. Ozkirimli, Co-encapsulation of isoniazid and rifampicin in liposomes and characterization of liposomes by derivative spectroscopy, Int. J. Pharm, 271 (2004) 115–123.

[12] H. Ferreira, M. Lúcio, B. de Castro, P. Gameiro, J.L.F.C. Lima, S. Reis, Partition and location of nimesulide in EPC liposomes: a spectrophotometric and fluorescence study, Anal. Bioanal. Chem, 377 (2003) 293–298.

[13] J.R. Lakowicz, B.R. Masters, Principles of Fluorescence Spectroscopy, Third Edition, J. Biomed. Opt, 13 (2008) 029901–029901–2.
[14] WHO, Global Tuberculosis Report 2012, World Health Organization, 2013.
[15] L. Jordao, O.V. Vieira, Tuberculosis: new aspects of an old disease, Int. J. Cell Biol, 2011 (2011) 403623.
[16] D. Dube, G.P. Agrawal, S.P. Vyas, Tuberculosis: from molecular pathogenesis to effective drug carrier design, Drug Discov. Today, 17 (2012) 760–773.
[17] J. Pieters, Mycobacterium tuberculosis and the macrophage: maintaining a balance, Cell Host Microbe, 3 (2008) 399–407.
[18] S.H.E. Kaufmann, How can immunology contribute to the control of tuberculosis? Nat. Rev. Immunol, 1 (2001) 20–30.
[19] J. Chan, J. Flynn, The immunological aspects of latency in tuberculosis, Clin. Immunol, 110 (2004) 2–12.
[20] M.P. Golden, H.R. Vikram, Extrapulmonary tuberculosis: an overview, Am. Fam. Physician, 72 (2005) 1761–1768.
[21] S.K. Sharma, A. Mohan, Extrapulmonary tuberculosis, Indian J. Med. Res, 120 (2004) 316–353.
[22] S. Singh, Tuberculosis, Curr. Anaesth. Crit. Care, 15 (2004) 165–171.
[23] M.S. Glickman, W.R. Jacobs, Microbial pathogenesis of Mycobacterium tuberculosis: dawn of a discipline, Cell, 104 (2001) 477–485.
[24] S.D. Lawn, A.I. Zumla, Tuberculosis, Lancet, 378 (2011) 57–72.
[25] C. Astarie-Dequeker, J. Nigou, C. Passemar, C. Guilhot, The role of mycobacterial lipids in host pathogenesis, Drug Discov. Today Dis. Mech, 7 (2010) e33–e41.
[26] J.L. Flynn, J. Chan, Immune evasion by Mycobacterium tuberculosis: living with the enemy, Curr. Opin. Immunol, 15 (2003) 450–455.
[27] B.M. Saunders, W.J. Britton, Life and death in the granuloma: immunopathology of tuberculosis, Immunol. Cell Biol, 85 (2007) 103–111.
[28] J.G. Pasipanodya, T. Gumbo, A new evolutionary and pharmacokinetic-pharmacodynamic scenario for rapid emergence of resistance to single and multiple anti-tuberculosis drugs, Curr. Opin. Pharmacol, 11 (2011) 457–463.
[29] Y. Zhang, K. Post-Martens, S. Denkin, New drug candidates and therapeutic targets for tuberculosis therapy, Drug Discov. Today, 11 (2006) 21–27.
[30] M. Pinheiro, M. Lúcio, J.L.F.C. Lima, S. Reis, Liposomes as drug delivery systems for the treatment of TB, Nanomedicine (London), 6 (2011) 1413–1428.
[31] S. Chouchane, I. Lippai, R.S. Magliozzo, Catalase-peroxidase (Mycobacterium tuberculosis KatG) catalysis and isoniazid activation, Biochemistry, 39 (2000) 9975–9983.
[32] C. Becker, J.B. Dressman, G.L. Amidon, H.E. Junginger, S. Kopp, K.K. Midha, V.P. Shah, S. Stavchansky, D.M. Barends, International Pharmaceutical Federation, Groupe BCS, Biowaiver monographs for immediate release solid oral dosage forms: isoniazid, J. Pharm. Sci, 96 (2007) 522–531.
[33] S.S. Kadam, Principles of Medicinal Chemistry, 18th ed. Nirali Prakashan, 2008.
[34] H. van der Lijke, The determination of small hydrophilic pharmaceuticals in blood serum, (2011).
[35] D.S. Wishart, C. Knox, A.C. Guo, D. Cheng, S. Shrivastava, D. Tzur, B. Gautam, M. Hassanali, DrugBank: a knowledgebase for drugs, drug actions and drug targets, Nucleic Acids Res, 36 (2008) D901–6.
[36] C. Vilchèze, W.R. Jacobs, The mechanism of isoniazid killing: clarity through

the scope of genetics, Annu. Rev. Microbiol, 61 (2007) 35–50.
[37] D.A. Rozwarski, G.A. Grant, D.H. Barton, W.R. Jacobs, J.C. Sacchettini, Modification of the NADH of the isoniazid target (InhA) from Mycobacterium tuberculosis, Science, 279 (1998) 98–102.
[38] B. Lei, C.J. Wei, S.C. Tu, Action mechanism of antitubercular isoniazid Activation by Mycobacterium tuberculosis KatG, isolation, and characterization of inha inhibitor, J. Biol. Chem, 275 (2000) 2520–2526.
[39] L.S. Hui, H.L. Cheng, T.L. Hui, N.A. Mohamad, A.N.D. Yazid, G.L. Harn, Antituberculosis, WebmedCentral Pharmaceutical Sciences, 2 (2011).
[40] R.J. White, G.C. Lancini, L.G. Silvestri, Mechanism of action of rifampin on Mycobacterium smegmatis, J. Bacteriol, 108 (1971) 737–741.
[41] A. Feklistov, V. Mekler, Q. Jiang, L.F. Westblade, H. Irschik, R. Jansen, A. Mustaev, S.A. Darst, R.H. Ebright, Rifamycins do not function by allosteric modulation of binding of Mg2+ to the RNA polymerase active center, Proceedings of the National Academy of Sciences, 105 (2008) 14820–14825.
[42] T.A. Wichelhaus, V. Schäfer, V. Brade, B. Böddinghaus, Molecular characterization of rpoB mutations conferring cross-resistance to rifamycins on methicillin-resistant Staphylococcus aureus, Antimicrob. Agents Chemother, 43 (1999) 2813–2816.
[43] A.L. Plant, Supported hybrid bilayer membranes as rugged cell membrane mimics, Langmuir, 15 (1999) 5128–5135.
[44] M. Aktas, M. Wessel, S. Hacker, S. Klüsener, J. Gleichenhagen, F. Narberhaus, Phosphatidylcholine biosynthesis and its significance in bacteria interacting with eukaryotic cells, Eur. J. Cell Biol, 89 (2010) 888–894.
[45] M.S. BRETSCHER, Asymmetrical Lipid Bilayer Structure for Biological Membranes : Abstract : Nature, Nature, 236 (1972) 11–12.
[46] R. Koynova, M. Caffrey, Phases and phase transitions of the phosphatidylcholines, BBA-Rev. Biomembranes, 1376 (1998) 91–145.
[47] S. Garcia-Manyes, G. Oncins, F. Sanz, Effect of temperature on the nanomechanics of lipid bilayers studied by force spectroscopy, Biophys. J, 89 (2005) 4261–4274.
[48] D.A. Brown, E. London, Structure and origin of ordered lipid domains in biological membranes, J. Membr. Biol, 164 (1998) 103–114.
[49] D. Lichtenberg, H. Ahyayauch, A. Alonso, F.M. Goñi, Detergent solubilization of lipid bilayers: a balance of driving forces, Trends Biochem. Sci, 38 (2013) 85–93.
[50] G. Ma, H.C. Allen, DPPC Langmuir Monolayer at the Air–Water Interface: Probing the Tail and Head Groups by Vibrational Sum Frequency Generation Spectroscopy, Langmuir, 22 (2006) 5341–5349.
[51] Y. Malam, M. Loizidou, A.M. Seifalian, Liposomes and nanoparticles: nanosized vehicles for drug delivery in cancer, Trends Pharmacol. Sci, 30 (2009) 592–599.
[52] R.P. Richter, R. Bérat, A.R. Brisson, Formation of solid-supported lipid bilayers: an integrated view, Langmuir, 22 (2006) 3497–3505.
[53] R.L. Owen, J.K. Strasters, E.D. Breyer, Lipid vesicles in capillary electrophoretic techniques: characterization of structural properties and associated membrane-molecule interactions, Electrophoresis, 26 (2005) 735–751.
[54] G.P. van Balen, C.A.M. Martinet, G. Caron, G. Bouchard, M. Reist, P.-A. Carrupt, R. Fruttero, A. Gasco, B. Testa, Liposome/water lipophilicity: methods,

information content, and pharmaceutical applications, Med. Res. Rev, 24 (2004) 299–324.
[55] D. Lichtenberg, Y. Barenholz, Liposomes: preparation, characterization, and preservation, Method. Biochem. Anal, 33 (1988) 337–462.
[56] G. Chimote, R. Banerjee, Effect of mycolic acid on surface activity of binary surfactant lipid monolayers, J. Colloid Interf. Sci, 328 (2008) 288–298.
[57] M. Pinheiro, J.J. Giner-Casares, M. Lúcio, J.M. Caio, C. Moiteiro, J.L.F.C. Lima, S. Reis, L. Camacho, Interplay of mycolic acids, antimycobacterial compounds and pulmonary surfactant membrane: A biophysical approach to disease, Biochim. Biophys. Acta, 1828 (2013) 896–905.
[58] G. Chimote, R. Banerjee, In vitro evaluation of inhalable isoniazid-loaded surfactant liposomes as an adjunct therapy in pulmonary tuberculosis, J. Biomed. Mater. Res-A, 94 (2010) 1–10.
[59] C. Nunes, G. Brezesinski, D. Lopes, Lipid–Drug Interaction: Biophysical Effects of Tolmetin on Membrane Mimetic Systems of Different Dimensionality, J. Phys Chem.-USA, 115 (2011) 12615–12623.
[60] M. Pinheiro, M. Arêde, J.M. Caio, C. Moiteiro, M. Lúcio, S. Reis, Drug-membrane interaction studies applied to N'-acetyl-rifabutin, Eur. J. Pharm. Biopharm, (2013).
[61] J. Brittes, M. Lúcio, C. Nunes, J.L.F.C. Lima, S. Reis, Effects of resveratrol on membrane biophysical properties: relevance for its pharmacological effects, Chem. Phys. Lipids, 163 (2010) 747–754.
[62] N. Michel, A.-S. Fabiano, A. Polidori, R. Jack, B. Pucci, Determination of phase transition temperatures of lipids by light scattering, Chem. Phys. Lipids, 139 (2006) 11–19.
[63] J.H. Lin, A.Y.H. Lu, Role of Pharmacokinetics and Metabolism in Drug Discovery and Development, Pharmaceutical Sciences, 49 (1997) 403–449.
[64] C.E. Barry, R.A. Slayden, A.E. Sampson, R.E. Lee, Use of genomics and combinatorial chemistry in the development of new antimycobacterial drugs, Biochem. Pharmacol, 59 (2000) 221–231.
[65] M. Pinheiro, M. Arêde, C. Nunes, J.M. Caio, Differential Interactions of Rifabutin with Human and Bacterial Membranes: Implication for Its Therapeutic and Toxic Effects, J. Med. Chem, 56 (2013) 417–426.
[66] M. Lúcio, C. Nunes, D. Gaspar, K. Gołębska, M. Wisniewski, J.L.F.C. Lima, G. Brezesinski, S. Reis, Effect of anti-inflammatory drugs in phosphatidylcholine membranes: A fluorescence and calorimetric study, Chem. Phys. Lett, 471 (2009) 300–309.
[67] A.N. Dickey, R. Faller, How alcohol chain-length and concentration modulate hydrogen bond formation in a lipid bilayer, Biophys. J, 92 (2007) 2366–2376.
[68] C. Pereira-Leite, C. Carneiro, J.X. Soares, C. Afonso, C. Nunes, M. Lúcio, S. Reis, Biophysical characterization of the drugâ€“membrane interactions: The case of propranolol and acebutolol, Eur. J. Pharm. Biopharm, 84 (2013) 183–191.
[69] A.P. Demchenko, Y. Mély, G. Duportail, A.S. Klymchenko, Monitoring biophysical properties of lipid membranes by environment-sensitive fluorescent probes, Biophys. J, 96 (2009) 3461–3470.
[70] J. Repáková, J.M. Holopainen, M.R. Morrow, M.C. McDonald, P. Capková, I. Vattulainen, Influence of DPH on the structure and dynamics of a DPPC bilayer, Biophys. J, 88 (2005) 3398–3410.
[71] A.M.S. Cardoso, H. Faneca, J.A.S. Almeida, A.A.C.C. Pais, E.F. Marques, M.C.P. de Lima, A.S. Jurado, Gemini surfactant dimethylene-1,2-

bis(tetradecyldimethylammonium bromide)-based gene vectors: A biophysical approach to transfection efficiency, BBA-Biomembranes, 1808 (2011) 341–351.
[72] C. Nunes, G. Brezesinski, C. Pereira-Leite, J.L.F.C. Lima, S. Reis, M. Lúcio, NSAIDs interactions with membranes: a biophysical approach, Langmuir, 27 (2011) 10847–10858.
[73] M.K. Jain, N.M. Wu, Effect of small molecules on the dipalmitoyl lecithin liposomal bilayer: III Phase transition in lipid bilayer - Springer, J. Membr. Biol, 34 (1977) 157–201.
[74] R. Pignatello, T. Musumeci, L. Basile, C. Carbone, G. Puglisi, Biomembrane models and drug-biomembrane interaction studies: Involvement in drug design and development, J. Pharm. Bioallied Sci, 3 (2011) 4–14.